Main Manuscript and Supporting information for

CyAbrB2 is a nucleoid-associated protein in *Synechocystis* controlling hydrogenase expression during fermentation

Ryo Kariyazono[1] and Takashi Osanai[1]*

[1]School of Agriculture, Meiji University

*Takashi Osanai

Postal address: 1-1-1 Higashimita, Tama-ku, Kawasaki, Kanagawa 214-8571, Japan

Telephone/Fax: +81-44-934-7103

Email: tosanai@meiji.ac.jp

Author Contributions: RK and TO designed the study; RK performed the study; RK analyzed the data; RK and TO wrote the paper

Competing Interest Statement: The authors declare no conflict of interest.

Classification:

Major: Biological sciences

Minor: Plant Biology

Keywords: cyanobacteria, transcription, microoxic response, hydrogenase, nucleoid-associated protein, sigma factor

This PDF file includes:

Main Text

Figures 1 to 5

Table 1

Figures S1 to S7

Tables S1 to S4

Abstract

The *hox* operon in *Synechocystis* sp. PCC 6803, encoding bidirectional hydrogenase responsible for H_2 production, is transcriptionally upregulated under microoxic conditions. Although several regulators for *hox* transcription have been identified, their dynamics and higher-order DNA structure of *hox* region in microoxic conditions remain elusive. We focused on key regulators for the *hox* operon: cyAbrB2, a conserved regulator in cyanobacteria, and SigE, an alternative sigma factor. Chromatin immunoprecipitation-sequencing revealed that cyAbrB2 binds to the *hox* promoter region under aerobic conditions, with its binding being flattened in microoxic conditions. Concurrently, SigE exhibited increased localization to the *hox* promoter under microoxic conditions. Genome-wide analysis revealed that cyAbrB2 binds broadly to AT-rich genome regions and represses gene expression. Moreover, we demonstrated the physical interactions of the *hox* promoter region with its distal genomic loci, and the interactions are lowered in microoxic conditions. In the absence of cyAbrB2, the interactions stayed low both in aerobic and microoxic conditions. From these results, we propose that cyAbrB2 is a cyanobacterial nucleoid-associated protein (NAP), modulating chromosomal conformation, which blocks RNA polymerase from the *hox* promoter in aerobic conditions. We further infer that cyAbrB2, with altered localization pattern upon microoxic conditions, modifies chromosomal conformation in microoxic conditions, which allows SigE-containing RNA polymerase to access the *hox* promoter. The coordinated actions of this NAP and the alternative sigma factor are crucial for the proper *hox* expression in microoxic conditions. Our results

46 highlight the impact of cyanobacterial chromosome conformation and NAPs on transcription, which have

47 been insufficiently investigated.

48

49

50 **Introduction**

51 Cyanobacteria carry out oxygenic photosynthesis but sometimes experience microoxic conditions during

52 the night. Subsequently, cyanobacteria perfrom fermentation, using glycolytic products as electron

53 acceptors. (1). Cyanobacteria have multiple fermentation pathways according to the environment. For

54 example, the freshwater living cyanobacterium *Synechocystis* sp. PCC 6803 (hereafter referred to as

55 *Synechocystis*) produces acetate, lactate, dicarboxylic acids, and hydrogen (1, 2). Genetic manipulations on

56 *Synechocystis* have demonstrated that modulating the expression of certain enzymes can alter fermentative

57 metabolic flow (3, 4). This provides evidence that transcription regulates the fermentative pathway.

58 Hydrogen has attracted significant attention among other cyanobacterial bioproducts owing to its potential

59 as a biofuel. Bidirectional hydrogenase is a key enzyme for H_2 production from protons (5) and is

60 commonly found in cyanobacteria (6). Cyanobacterial hydrogenase comprises five subunits (HoxEFUHY)

61 containing nickel and Fe-S clusters (7). This enzyme can utilize NADH, reduced ferredoxin, and flavodoxin

62 as substrates (8). Hydrogenase can also use excess electrons from the photosynthetic electron transport

63 chain, but photosystem II-generated oxygen can inhibit its activity (9). Another metal-ion-harboring and

64 O_2-sensitive enzyme, pyruvate-ferredoxin oxidoreductase (PFOR), oxidizes pyruvate to produce acetyl-
65 CoA during fermentation. PFOR works coordinatedly with hydrogenase to reduce ferredoxin, which
66 hydrogenase uses as an electron donor (8, 10). Despite their O_2 sensitivity, hydrogenase and PFOR work
67 under mixotrophic (i.e., aerobic) conditions (11, 12). Therefore, uncontrolled expression of *hox* operon and
68 *nifJ* may hamper metabolism under photosynthetic conditions or shorten the supply of inorganic cofactors.
69 Thus, transcriptional regulation in response to the environment is essential for optimal energy cost
70 performance.

71 Promoter recognition by RNA polymerases is an essential step in transcriptional regulation. Sigma factors,
72 subunits of RNA polymerase, recognize core promoter sequences. Transcription factors can also bind to
73 promoter regions to suppress or promote RNA polymerase transcription. As well as recruitment or blocking
74 of RNA polymerase, some transcriptional factors, known as Nucleoid-associated proteins (NAPs),
75 modulate chromosomal conformation to regulate transcription (13). NAPs are common in bacteria, but
76 cyanobacterial NAPs remain unidentified, and higher order of DNA structure in cyanobacteria is yet to be
77 shown. A recent study suggested that the manipulation of chromosomal supercoiling impacts transcriptional
78 properties in cyanobacteria (14). There is room for consideration of NAPs modulating chromosomal
79 conformation and regulating expression in cyanobacteria.

80 In *Synechosysits*, the coding genes of HoxEFUHY form a single operon (sll1220–1226), while PFOR is
81 encoded in the *nifJ* (sll0741) gene. Both *hox* and *nifJ* operons are highly expressed under microoxic

82 conditions (15). Genetic analysis has revealed that multiple global transcriptional regulators control *hox*

83 and *nifJ* expression. Sigma factor SigE (Sll1689) promotes the expression of *hox* and *nifJ* operons (16, 17),

84 while transcription factor cyAbrB2 (Sll0822) represses them (18, 19). Positive regulators for the *hox* operon

85 include LexA (Sll1626) and cyAbrB1 (Sll0359) (20–22).

86 SigE, an alternative sigma factor, controls the expression of genes involved in glycogen catabolism and

87 glycolysis, as well as PFOR/*nifJ* and hydrogenase (16). SigE shares a high amino acid sequence homology

88 with the primary sigma factor SigA, which is responsible for transcribing housekeeping and photosynthetic

89 genes (23). A ChIP-seq study revealed that, while most SigE-binding sites are the same as SigA, SigE

90 exclusively occupies the promoters of glycogen catabolism and glycolysis (24).

91 CyAbrB2 and its homolog cyAbrB1 are transcription factors highly conserved in cyanobacteria. For

92 example, cyAbrB homologs in *Anabaena* sp. PCC7120 is involved in heterocyst formation (25). CyAbrB2

93 in *Synechocystis* regulates the expression of several genes involved in carbon metabolism, nitrogen

94 metabolism, and cell division (19, 26, 27). CyAbrB2 binds to the *hox* promoter *in vitro* and represses its

95 expression *in vivo* (18). CyAbrB1, an essential gene, physically interacts with the cyAbrB2 protein (28)

96 and binds the *hox* promotor region *in vitro* to promote its expression (20).

97 To explore the dynamics of those transcription factors governing the expression of *hox* operon, we

98 conducted a time-course analysis of the transcriptome and ChIP-seq of SigE and cyAbrB2. Our ChIP-seq

99 and transcriptome analysis showed the NAPs-like nature of cyAbrB2, which prompted us to conduct

100 chromosomal conformation capture assay. 3C analysis revealed the physical interaction between the *hox*
101 promoter region and its downstream and upstream genomic region in the aerobic condition, and that the
102 interaction decreased upon entry to the microoxic condition. Furthermore those interactions in the
103 Δ*cyabrB2* mutant were low both in aerobic and microoxic conditions. From those experiments, we propose
104 that cyAbrB2 modulates chromosomal conformation like NAPs, allowing access to the SigE-containing
105 RNA polymerase complex on the *hox* promoter, by which the *hox* operon achieves distinct expression
106 dynamics. Chromosomal conformation of bacteria is a growing area of interest, and the findings of this
107 study have brought insight into the transcriptional regulation of cyanobacteria.

108 **Results**

109 **Transcriptomes on entry to dark microoxic conditions**

110 To understand transcriptional regulation under microoxic conditions, we conducted a time-course
111 transcriptome capturing aerobic and microoxic conditions at 1-, 2-, and 4-hours timepoints (Figure 1A).
112 Gene set enrichment analysis based on KEGG pathway revealed that many biological pathways, including
113 photosynthesis and respiration (oxidative phosphorylation), were downregulated under microoxic
114 conditions compared to aerobic conditions (Figure 1B). Upregulated pathways included butanoate
115 metabolism and two-component systems, but the actual cyanobacterial catabolic pathway differed slightly
116 from that described in the KEGG pathway. Within 1 hour of switching from aerobic to microoxic conditions,
117 the expression levels of 508 genes increased more than 2-fold. Furthermore, genes with increased

118 expression levels were classified into four based on the time-course (Figure 1C). Of the 508 genes, 28 were
119 termed “transiently upregulated genes” due to their decreased expression upon the comparison of 1- and 4-
120 hours incubation under microoxic conditions (log2 fold change < −0.5), and 119 were termed “continuously
121 upregulated genes.”, which continuously increased between 1- and 4-hours incubation under microoxic
122 conditions (log2-fold change > 0.5). Other than 508 genes 2-fold upregulated within 1 hour, 28 genes
123 showed more than 4-fold increment within 4 hours but not upregulated within 1 hour. We combined those
124 "Late upregulated genes" with 508 genes and referred to as "All upregulated genes" in the subsequent
125 analysis (Figure 1C). Mapping the classified genes to central carbon metabolism revealed that *nifJ* encoding
126 PFOR and *hox* operon encoding a bidirectional hydrogenase complex were transiently upregulated (Figure
127 1D and Table 1). RTqPCR verified the transient expression of *hoxF*, *hoxH,* and *nifJ* (Figure S1).

128 **SigE and cyAbrB2 control the expression of transiently upregulated genes**

129 The functional correlation between hydrogenase and PFOR, encoded by the *hox* operon and *nifJ,* suggests
130 that transient upregulation has physiological significance. We focused on transiently upregulated genes and
131 attempted to reveal the regulatory mechanism underlying transient upregulation. While SigE promotes the
132 expression of *hox* and *nifJ*, cyAbrB2 represses them (16, 18, 19). We confirmed that the deletion of *sigE*
133 and *cyabrb2* (Δ*sigE* and Δ*cyabrb2*, respectively) affected the expression of *hoxF*, *hoxH*, and *nifJ* by RT-
134 qPCR (Figure S1). Thus, we conducted a time-course transcriptome analysis of Δ*sigE* and Δ*cyabrb2* under
135 aerobic conditions and after 1- and 2-hours cultivation in dark microoxic conditions (Figures 2A and S2A).

136 The transcriptome data confirmed that SigE and cyAbrB2 regulated *hox* operon expression (Figure 2B). At
137 each time point, we searched for differentially expressed genes (DEGs) between mutants and wildtype with
138 a more than 2-fold expression change and a false discovery rate (FDR) less than 0.05. We found that deleting
139 *sigE* or *cyabrb2* preferentially affected the expression of transiently upregulated genes, not limited to *hox*
140 and *nifJ* operons (Figures 2C and 2D). Interestingly, *cyabrb2* deletion resulted in the upregulated expression
141 of transient genes under aerobic conditions, in contrast to 1-hour cultivation under microoxic conditions
142 (Figure 2C).

143 **Genome-wide analysis of cyAbrB2, cyAbrB1, and SigE via ChIP-seq**

144 To decipher the regulatory mechanism of transiently upregulated genes, we must first comprehend the
145 fundamental features and functions of these transcriptional regulators. Therefore, a genome-wide survey of
146 cyAbrB2 and SigE occupation (Figures S2 and S3) combined with transcriptome data was done.
147 Specifically, we generated a *Synechocystis* strain in which cyAbrB2 was epitope-tagged and performed a
148 ChIP-seq assay under aerobic and microoxic conditions (Figures S2B and S2C). SigE-tagged strains
149 previously constructed and analyzed elsewhere were also employed (24). The primary sigma factor SigA
150 was also analyzed to determine SigE-specific binding. In addition to cyAbrB2, we tagged and analysed
151 cyAbrB1, which is the interactor of cyAbrB2 and positively regulates the *hox* operon.

152 **CyAbrB2 binds to long tracts of the genomic region and suppresses genes in the binding region**

153 The ChIP-seq data showed that cyAbrB2 bound to long tracts of the genomic region with lower GC

154 content than the whole genome *Synechocystis* (Figures 3A and 3B). Vice versa, regions exhibiting lower
155 GC contents showed a greater binding signal of cyAbrB2 (Figure 3C). This correlation was not a systematic
156 bias of next-generation sequencing because the binding signals of SigE, SigA, and control showed no
157 negative correlation to GC contents (Figure S4A). The binding regions of cyAbrB2 called by peak-caller
158 covered 15.7% of the entire genome length. 805 of 3614 genes overlapped with cyAbrB2 binding regions,
159 and almost half (399 of 805 genes) were entirely covered by cyAbrB2 binding regions. The cyAbrB2
160 binding regions included 80 of 125 insertion sequence elements (Figure 3D). Comparison with the
161 transcriptome of Δ*cyabrB2* revealed cyAbrB2 tended to suppress the genes overlapping with its binding
162 regions under aerobic conditions (Figures 3A and 3E). A survey of the genomic localization of cyAbrB1
163 under aerobic conditions revealed that cyAbrB1 and cyAbrB2 shared similar binding patterns (Figures 3A
164 and S4C). Due to the essentiality of cyAbrB1, we did not perform transcriptome analysis on a cyAbrB1-
165 disrupted strain.

166 **Localization of cyAbrB2 became blurry under the microoxic condition**

167 When cells entered microoxic conditions, the relative ChIP-seq signals in the cyAbrB2 binding regions
168 slightly declined (Figure S5A). However, the signal change did not necessarily indicate that cyAbrB2
169 binding declined under microoxic conditions because the relative signal was normalized by total reads of
170 immunoprecipitation and input. Rather, the cyAbrB2 binding pattern became uniform when the cells
171 entered microoxic conditions. Notably, the total quantities of precipitated DNA by tagged cyAbrB2 did not

172 decrease, and qPCR confirmed that the cyAbrB2 binding signal increased in all positions tested (Figure
173 S5B and S5C). The protein amount of cyAbrB2 was not altered on entry to the mircooxic condition (Figure
174 S5D).

175 **CyAbrB2 binds to transiently upregulated genes**

176 The binding regions of cyAbrB2 overlapped 17 of 28 transiently upregulated genes, showing significant
177 enrichment from all upregulated genes (Figure 3F). While cyAbrB2 covered the entire length of insertion
178 sequences and unknown proteins, its binding positions on other transient genes were diverse (Figure 3G).
179 Specifically, the *hox* and *nifJ* operons had two distinct binding regions located at the transcription start sites
180 (TSSs) and middle of operons, the *pntAB* operon had two binding regions in the middle and downstream
181 of the operon, and the *nrtABCD* operon had one binding region downstream of the operon (Figure 3H).
182 Upon entry into microoxic conditions, the cyAbrB2 binding signal around the transiently upregulated genes
183 became less specific, consistent with the general tendency.

184 **Sigma factors SigE and SigA are excluded from cyAbrB2 binding regions regardless of GC contents**

185 We searched for SigE and SigA binding sites under aerobic and microoxic conditions (Figures 4A and 4B,
186 left and right). The SigE and SigA peaks identified in this study predominantly covered the previously
187 identified peaks (Figure S2D), reproducing the previous study's conclusion (24); i.e., SigE and the primary
188 sigma factor SigA share localization on the promoters of housekeeping genes, but SigE exclusively binds
189 to the promoters of its dependent genes. SigE and SigA binding peaks were significantly excluded from the

190 cyAbrB2 binding regions (Figure 4C), and signals in cyAbrB2 binding regions were weaker than those in
191 cyAbrB2-free regions (Figure 4D). As cyAbrB2 prefers AT-rich regions, we examined whether the peak
192 summits of SigE and SigA were located in regions with high GC contents. Unexpectedly, no correlation
193 was found between the GC content and binding signals of SigE and SigA (Figures S4A and S4B). Thus,
194 SigA and SigE are excluded from cyAbrB2 binding regions regardless of GC contents.

195 **Dynamics of sigma factors upon exposure to the microoxic condition**

196 When cells entered microoxic conditions, the binding signals of SigA and SigE were changed, although
197 most of their peaks observed under aerobic conditions were present under microoxic conditions (Figure
198 4A). Next, we focused on sigma factor dynamics in transiently upregulated genes. SigE, but not SigA, binds
199 at the TSS of *pntAB* under aerobic and microoxic conditions (Figure 4E top). SigE binding summits were
200 not identified at the TSSs of the *hox* and *nifJ* operons under aerobic conditions. However, the SigE-specific
201 binding summit appeared at the TSS of *nifJ* when cells entered microoxic conditions (Figure 4E middle).
202 A bimodal peak of SigE was observed at the TSS of the *hox* operon, although the peak caller failed to
203 recognize it as two peaks (Figure 4E bottom panel). One side of the bimodal peak marked with an arrow in
204 Figure 4E lacked SigA binding. SigE binding without SigA on the promoters of *hox*, *nifj*, and *pntAB* is
205 consistent with their SigE-dependent expression (Figure 2B).

206 **CyAbrB2-dependent and independent chromatin conformation around *hox* operon**

207 We have shown that cyAbrB2 broadly binds to AT-rich genomic regions, including insertion element

208 sequences, and represses expression (Figures 3B and 3D). This is functionally similar to the NAPs (13),

209 which makes us hypothesize that cyAbrB2 modulates chromosomal conformation. Therefore, we

210 conducted the chromatin conformation capture (3C) assay against wildtype and *cyabrb2*Δ strain at aerobic

211 and microoxic conditions (1hr and 4hr). qPCR was performed with unidirectional primer sets, where the

212 genomic fragment containing *hox* operon (hereinafter *hox* fragment) was used as bait (Figure 5A). We then

213 observed that the *hox* fragment interacted with its distal downstream (~25 kbp) region and proximal

214 upstream (~10 kbp) region in the aerobic condition (Figure 5B and 5C, locus(c) and (j)). Those interactions

215 were detected both in wildtype and Δ*cyabrb2*. However, the interaction frequency between the *hox*

216 fragment and its distal downstream was higher in wildtype than Δ*cyabrb2* (Figure S7 locus(c)).

217 **CyabrB2 mediates chromatin conformation changes upon microoxic conditions.**

218 When the wildtype cells entered the microoxic condition, the *hox* fragment diminished its interaction with

219 its distal downstream and proximal upstream region (Figure 5B locus(c) and (j)). By contrast, the interaction

220 frequency in Δ*cyabrb2* mutant were low and unchanged in the aerobic and microoxic conditions. While the

221 interaction scores exhibit considerable variability, the individual data over time demonstrate declining

222 trends of the wildtype at locus (c) and (j) (Figure S7). Furthermore, both wildtype and Δ*cyabrb2* mutant

223 showed increased interaction with the proximal downstream fragments on entry to the microoxic conditions

224 (Figure 5B and 5C, locus (f),(g),(h)). In the wildtype cells, the interaction with locus (g) was transiently

225 elevated at 1 hour of the microoxic condition but decreased to the aerobic level at 4 hours. In summary, 3C

226 analysis demonstrated cyAbrB2-dependent and independent dynamics of chromosomal conformation

227 around the *hox* operon in response to the microoxic condition (Figure 5D).

228 **Discussion**

229 **Physiological significance of transient upregulation of *hox* and *nifJ* operons**

230 The transcriptional upregulation of fermentative genes in response to the microoxic condition is adaptive

231 for energy acquisition. Our time-course transcriptome showed upregulation of several genes involved in

232 catabolism upon exposure to the microoxic condition. The transient upregulation of *hox* and *nifJ* operons

233 is distinctive among them (Figure 1D).

234 The reason for transient upregulation may be the resource constraints of inorganic cofactors and the

235 reusability of fermentative products. Hydrogenase and PFOR (the product of *nifJ* gene) have iron–sulfur

236 clusters, and hydrogenase requires nickel for its activity (29, 30). Continuous expression of the *hox* operon

237 should be futile under physiological conditions, as the overexpression of *hoxEFUYH* and *hypABDCEF*

238 (hydrogenase maturation factors) does not yield a proportional increase in hydrogenase activity without an

239 adequate nickel supply (31). Furthermore, hydrogenase-produced H_2 is diffusive and thus difficult to store

240 and reuse as reducing power when cells return to aerobic conditions. Unlike hydrogen fermentation, the

241 reverse tricarboxylic acid (rTCA) cycle produces dicarboxylic acids, which are reusable for generating

242 NADPH via the TCA cycle under aerobic conditions (32). However, adding bicarbonate to

243 phosphoenolpyruvate (PEP) is a rate-limiting step in the rTCA cycle (33). Hydrogenase may favor

244 fermentation initiation since it uses only protons as a substrate, and the rTCA cycle may become active

245 subsequently. In fact, *citH*/*mdh* (sll0891) encoding a key enzyme of the rTCA cycle was classified as

246 continuously upregulated genes in this study (Figure 1D).

247 **Mechanisms for transient expression mediated by SigE and cyAbrB2**

248 SigE and cyAbrB2 can independently contribute to the transient transcriptional upregulation. This is

249 evident as the single mutants, Δ*sigE* or Δ*cyabrb2*, maintained transient expression of *hoxF* and *nifJ* (Figure

250 S1). Here we discuss the cyAbrB2-mediated mechanism, then that of SigE will be discussed.

251 **Three types of the localization pattern and function of cyAbrB2**

252 Herein, we classified three types of binding patterns for cyAbrB2 based on the ChIP-seq data of cyAbrB2.

253 The first is that cyAbrB2 binds a long DNA tract covering the entire gene or operon, represented by the

254 insertion sequence elements. CyAbrB2 suppresses expression in this pattern, as shown in Figures 3D and

255 3E. In the second pattern, cyAbrB2 binds on promoter regions, such as *hox* operon and *nifJ*. Binding on

256 those promoters fluctuates in response to environmental changes, thus regulating expression. This pattern

257 also applies to the promoter of *sbtA* (Na^+/HCO_3^- symporter), as the previous study reported that cyAbrB2

258 is bound to the *sbtA* promoter in a CO_2 concentration-dependent manner (27). The last one is cyAbrB2

259 binding in the middle or downstream of operons. The middle of *hox*, *pntAB*, and *nifJ* operons and the

260 downstream of *nrt* operon are the cases (Figure 3G). Our data show that genes in the same operon separated

261 by the cyAbrB2 binding region behave differently. In particular, *pntB* is classified as the transiently

262 upregulated gene, while *pntA* is not, despite being in the same operon. This might be explained by the recent
263 study which reported that cyAbrB2 affects the stability of mRNA transcribed from its binding gene (34).
264 The cyAbrB2-mediated stability of mRNA may also account for the decrease in transcript from transient
265 upregulated genes at 4 hours of cultivation. Hereafter, we will focus on the mechanism of the second pattern,
266 regulation by cyAbrB2 on the promoter.

267 **Insights into transcriptional regulation of *hox* operon and *nifJ***

268 Genome-wide analysis indicates that the cyAbrB2-bound region blocks SigE and SigA (Figures 4C and
269 4D). This is presumably because sigma factors recognize the promoter as a large complex of RNA
270 polymerase. CyAbrB2 binds to the *hox and nifJ* promoter region and may inhibit access to RNA polymerase
271 complex under aerobic conditions. When cells entered microoxic conditions, the binding pattern of
272 cyAbrB2 on the *hox* and *nifJ* promoters got less specific, and SigE binding peaks on those promoters
273 became prominent (Figure 4E). Notably, cyAbrB2 ChIP efficiency at the *hox* promoter is higher in the
274 microoxic condition than in the aerobic condition (Figure S5C). Hence, the mechanism by which cyAbrB2
275 inhibits SigE-containing RNAP in the aerobic condition is not solely based on exclusion by occupancy.
276 Rather, it is plausible that chromosomal conformation change governed by cyAbrB2 provides SigE-
277 containing RNAP with access to the promoter region (Figure 5D).

278 **Chromosomal conformation in *hox* region changes according to the environmental change**

279 3C analysis demonstrated the interaction between the *hox* promoter and its distal genomic region, which

280 decreased on entry to the microoxic condition. CyAbrB2 mediates the interaction between the *hox* fragment
281 and the distal downstream region. The observed conformational change correlates with the expression of
282 the *hox* operon, though further investigations are needed to establish causality (Figures 5B and S7, locus
283 (f), (g), and (j)). A recent study demonstrated that manipulating the expression of topoisomerase, which
284 influence chromosomal conformational change through supercoiling, affect transcriptional properties in
285 cyanobacteria (14). Moreover, Song et al. pointed out that DNA looping may inhibit transcription in
286 cyanobacteria (34) because artificial DNA looping by the LacI repressor of *E. coli* can repress
287 cyanobacterial transcription (35). Thus, we infer conformation change detected by the present 3C
288 experiment regulates expression of *hox* operon.

289 **A possible mechanism for cyAbrB2-mediated chromosomal conformation**

290 The *hox* promoter region possesses the cyAbrB2 binding region, and locus (c) is adjacent to the cyAbrB2
291 binding region. Consequently, cyAbrB2 may mediate chromosomal conformation by bridging its binding
292 regions, as other NAPs do. However, no biochemical data mentioned the DNA bridging function of
293 cyAbrB2 in the previous studies (18, 26, 34). CyAbrB1, the homolog of cyAbrB2, may cooperatively work,
294 as cyAbrB1 directly interacts with cyAbrB2 (28), and their distribution is similar (Figure 3A). In the
295 microoxic condition, cyAbrB2 binding became blurry, which might reduce the specific interaction between
296 the *hox* region and locus (c). On the other hand, cyAbrB2 indirectly mediates interaction with its proximal
297 upstream region (Figure 5B, locus (j)), as this region is devoid of cyAbrB2 binding (Figure 5A locus (i) to

298 (l)).

299 **Generality for chromosomal conformation in cyanobacteria**

300 Our 3C analysis revealed that local chromosomal conformation changes upon entry to the microoxic
301 conditions (Figure 5D). As cyAbrB2 occupies about 15% of the entire genome and globally regulates gene
302 expression, cyAbrB2 likely governs the whole chromosomal conformation (Figure 5E). Furthermore, the
303 conformational changes occur in both AbrB2-dependent and AbrB2-independent manners. Cyanobacteria
304 face various environmental changes besides the microoxic condition, and there are potential NAPs in
305 cyanobacteria yet to be characterized. It is speculated that conformational change of the entire chromosome
306 occurs to deal with many environmental stresses.

307 **The sigE-mediated mechanism for the transient expression**

308 One possible SigE-mediated mechanism for transient expression is the post-transcriptional activation and
309 degradation of SigE in the dark; i.e., SigE is sequestered by binding to the H subunit of Magnesium-
310 chelatase under light conditions and released under dark (36), enabling acute transcription of *hox* operon
311 and *nifJ*. Transcripts of *sigE* were continuously downregulated in our time-course transcriptome, while *sigB*
312 (sll0306) and *sigC* (sll0184) were classified as continuous upregulated genes (Supplemental Table S1). It
313 is possible that upregulated SigB and SigC outcompete SigE in prolonged incubation under microoxic
314 conditions. Finally, SigE is degraded under dark within 24 hours (37).

315 Another reason for the microoxic specific expression may exist in the sequence of the *hox* promoter. We

316 previously determined the consensus sequence of -10 element for SigE regulon in the aerobic condition as

317 "TANNNT," where N is rich in cytosine (24). The -10 sequence of the *hox* promoter "TAACAA" (22)

318 deviates from the consensus, and no hexamer precisely fitting the consensus are found in the *nifJ* promoter.

319 This deviation can inhibit SigE from binding during aerobic conditions, aside from cyAbrB2-mediated

320 inhibition. Under the microoxic condition, transcription factors LexA (22) and Rre34 (15) may aid SigE

321 binding to the promoter of *hox* and *nifJ*, respectively. Overall, multiple environmental signals are integrated

322 into the *hox* and *nifJ* promoter through the cyAbrB2 and SigE dynamics.

323 **Materials and Methods**

324 **Bacterial strains and plasmids**

325 The glucose-tolerant strain of *Synechocystis* sp. PCC 6803 (38) was used as a wildtype strain in this study.

326 The *sigE* (sll1689)-disrupted strain (G50) was constructed in a previous study (16). Disruption and epitope-

327 tagging of *cyabrb1*(sll0359) and *cyabrb2*(sll0822) were performed by homologous double recombination

328 between the genome and PCR fragment (38). The resulting transformants were selected using three

329 passages on BG-11 plates containing 5 µg/mL kanamycin. Genomic PCR was used to confirm the insertion

330 of epitope tag fragments and gene disruption (Figure S2A). Supplemental Tables S2, S3, and S4 contain

331 the cyanobacterial strains, oligonucleotides, and plasmids used in this study.

332 **Aerobic and microoxic culture conditions**

333 For aerobic conditions, cells were harvested after 24 hours cultivation in HEPES-buffered BG-11_0 medium

334 (39), which was buffered with 20 mM HEPES-KOH (pH 7.8) containing 5 mM NH_4Cl under continuous

335 exposure to white light (40 μmol $m^{-2}s^{-1}$) and bubbled with air containing 1% CO_2 (final OD_{730} = 1.4–1.8).

336 For the dark microoxic culture, the aerobic culture cell was concentrated to an OD_{730} of 20 with the

337 centrifuge and resuspended in the culture medium. The concentrated cultures were poured into vials,

338 bubbled with N_2 gas, and sealed. The sealed vials were shaded and shaken at 30˚C for the described times.

339 **Antibodies and immunoblotting**

340 Sample preparation for immunoblotting was performed as previously described (24), and FLAG-tagged

341 proteins were detected by alkaline-phosphatase-conjugated anti-FLAG IgG (A9469, Sigma Aldrich, St.

342 Louis, MO) and 1-Step NBT/BCIP substrate solution (Thermo Fisher Scientific, Waltham, MA).

343 **RNA isolation**

344 Total RNA was isolated with ISOGEN (Nippon gene, Tokyo, Japan) following the manufacturer's

345 instructions and stored at −80˚C until use. The extracted RNA was treated with TURBO DNase (Thermo

346 Fisher Scientific) for 1 hour at 37˚C to remove any genomic DNA contamination. We confirmed that the

347 A260/A280 of the extracted RNA was >1.9 by NanoDrop Lite (Thermo Fisher Scientific). We prepared

348 triplicates for each timepoint for the RNA-seq library. RT-qPCR was performed as discribed elsewhere (37).

349 **ChIP assay**

350 Two biological replicates were used for each ChIP-seq experiment, and one untagged control ChIP was

351 performed. ChIP and qPCR analyses were performed using the modified version of a previous method (24).

352 FLAG-tagged proteins were immunoprecipitated with FLAG-M2 antibody (F1804 Sigma-Aldrich)
353 conjugated to protein G dynabeads (Thermo Fisher Scientific).

354 **Library preparation and next-generation sequencing**

355 For the ChIP-seq library, input and immunoprecipitated DNA were prepared into multiplexed libraries
356 using NEBNext Ultra II DNA Library Prep Kit for Illumina (New England Biolabs, Ipswich, MA). For the
357 RNA-seq library, isolated RNA samples were deprived of ribosomal RNA with Illumina Ribo-Zero Plus
358 rRNA Depletion Kit (Illumina, San Diego, CA) and processed into a cDNA library for Illumina with the
359 NEBNext Ultra II Directional RNA Library Prep Kit for Illumina (New England Biolabs). Dual-index
360 primers were conjugated with NEBNext Multiplex Oligos for Illumina (Set1, New England Biolabs). We
361 pooled all libraries, and the multiplexed libraries were dispatched to Macrogen Japan Inc. and subjected to
362 paired-end sequencing with HiSeqX. Adapter trimming and quality filtering of raw sequence reads were
363 conducted with fastp (ver. 0.21.0) (40) under default conditions. The paired-end sequences were mapped
364 onto the *Synechocystis* genome (ASM972v1) using Bowtie2 (41) (ver. 2.4.5 paired-end). Supplementary
365 Table S5 contains the read counts that passed via fastp quality control and were mapped by Bowtie2.

366 **RNA-seq analysis**

367 Mapped reads were counted by HT-seq count (ver. 2.0.2) (42) for the GFF file of ASM972v1, with the
368 reverse-strandedness option. EdgeR package (ver. 3.40.1) (43) was used to perform the differential
369 expression analysis. Fold changes in expression and FDR were used for gene classification. Supplemental

370 Table S6-S8 contains fold change in gene expression calculated by edgeR.

371 **Genome-wide analyses**

372 Peaks were called using the MACS3 program (ver. 3.0.0b1) (44). For paired-end reads for SigE, SigA,
373 and untagged control ChIP, narrow peaks were called with <1e−20 of the q-value cut-off and "--call-
374 summits" options. The peak summits from two replicates and the untagged control were merged if summits
375 were located within 40 bp of each other. Peak summits identified in both replicates but not in the control,
376 were considered for further analysis. The midpoint of the peak summits for the two merged replicates was
377 further analyzed.

378 Broad peak calling methods were applied to paired-end reads for cyAbrB2, cyAbrB1, and untagged
379 control ChIP using the "–broad" option, with a q-value cut-off of < 0.05 and a q-value broad cut-off of <
380 0.05. The intersection of broad peaks from two replicates, excluding those called by the control, was used
381 in subsequent analyses.

382 The positions of the TSS, including internal start sites, were obtained as reported by (45). The read count,
383 merging, and the intersection of the binding region were calculated using BEDTools (ver. 2.30.0) (46).
384 Supplemental Tables S9–S15 contain SigA and SigE peaks and the broad binding regions of cyAbrB2 and
385 cyAbrB1, respectively.

386 Binding signals in every 100 bp bin for scatter plots were calculated as (IP read counts within 100 bp
387 window) / (input read counts within 100 bp window) * (total input read counts/total IP read counts). GC

388 contents were calculated within 500 bp in 100 bp sliding windows by seqkit (ver. 2.3.0) (47).

389 **Genome extraction, digestion, and ligation for 3C assay**

390 A 3C assay was conducted based on the previous prokaryotic Hi-C experiment (48, 49), with certain steps

391 modified. To begin, *Synechocystis* were fixed with 2.5% formaldehyde for 15 minutes at room temperature.

392 Fixation was terminated by adding a final concentration of 0.5M of glycine, and cells were stored at -80˚C

393 until use. Fixed cells were disrupted using glass beads and shake master NEO (Bio Medical Science, Tokyo,

394 Japan), following the previous study's instructions for preparing cell lysate for ChIP. The lysates were

395 incubated with buffer containing 1mM Tris-HCl (pH7.5), 0.1mM EDTA, and 0.5% SDS for 10min at room

396 temperature, and 1% Triton X-100 quenched SDS. Genomes in the cell lysate were digested by 600U/mL

397 of HindIII (Takara Bio, Shiga, Japan) for 4 hours at 37˚C, and RNA in the lysate was simultaneously

398 removed by 50 µg/mL of RNaseA (Nippon genetics, Tokyo, Japan). The digestion was terminated by adding

399 1% SDS and 22 mM EDTA. The fill-in reaction and biotin labeling steps were omitted from the procedure.

400 The digested genomes were diluted by ligation buffer containing 1% triton-X100 to the final concentration

401 of approximately 1µg/mL and incubated for 10 min at room temperature. Ligation was performed with 2

402 U/mL of T4 DNA ligase (Nippon Gene) overnight at 16˚C. Crosslinking was reversed under 65˚C for 4

403 hours in the presence of 2.5 mg/mL of proteinase K (Kanto Chemical, Tokyo, Japan), and DNA was purified

404 with the phenol-chloroform method and ethanol precipitation method.

405 **Preparation of calibration samples for 3C qPCR**

406 Based on a previous study, calibration samples for possible ligated pairs were prepared in parallel with 3C
407 ligation (50). In brief, the purified genome of *Synechocystis* was digested by HindIII, and DNA was purified
408 with the phenol-chloroform and ethanol precipitation. Purified DNA was dissolved into the ligation buffer
409 at a concentration of about 600ng/μL and ligated with 2 U/mL of T4 DNA ligase at 16˚C overnight. As a
410 result, DNA ~600-fold condensed DNA than 3C samples were ligated.

411 **Quantification of crosslinking frequency for 3C assay**

412 Before the real-time PCR assay, we confirmed that each primer set amplified single bands in a ligation-
413 dependent manner by GoTaq Hot Start Green Master Mix (Promega, Madison, WI) (Figure S6). Real-time
414 PCR was performed with StepOnePlus (Applied Biosystems, Foster City, CA) and Fast SYBR Green
415 Master Mix (Thermo Fisher Scientific) according to the manufacturer's instructions. Interaction frequency
416 was calculated by ΔΔCt method using dilution series of calibration samples described above. We confirmed
417 each primer set amplified DNA fragment with a unique Tm value. The amount of the bait fragment
418 containing *hox* operon were quantified and used as an internal control. Supplemental Table S4 contains the
419 list of primers used in the 3C quantification. Interaction frequency for each primer position was calculated
420 as the relative abundance of ligated fragments against the calibration samples and normalized among
421 samples by internal control.

422 **Statistical analysis**

423 Statistical analyses were performed with R version 4.2.2 (51). The "fisher.test" function was used for

Fisher's exact test, and p-values < 0.05 were denoted as asterisks in the figure. Multiple comparisons of Fisher's exact test were conducted using "fisher. Multcomp" function in the RVAideMemoire package (52), where p-values were adjusted by the "fdr" method and FDRs <0.05 are shown in the figures. Multiple comparisons of the Wilcoxon-rank test were conducted by "pairwise.wilcox.test," and p-values were adjusted by the "fdr" method. Adjusted p-values < 0.05 are shown in the figure. The correlation coefficient was calculated with the "cor" function. Gene set enrichment analysis (GSEA) was performed by culsterPlofiler package (53) in R with p-value cut-off of 0.05. The enriched pathways detected by GSEA are listed in Supplemental Table S16.

Manuscript writing

We employed GPT-3.5 to refine the expression of the manuscripts.

Accession Numbers

Raw ChIP sequencing and RNA sequencing reads were deposited in the Sequence Read Archive (accession ID: PRJNA956842).

Declaration of interest

The authors declare no competing interests.

Acknowledgments

This study was supported by the following grants to T.O.: Grant-in-Aid for Scientific Research (B) (grant

no. 20H02905), JST-ALCA of the Japan Science and Technology Agency (grant number JPMJAL1306), and the Asahi Glass Foundation. We thank Dr. Kohki Yoshimoto for providing laboratory instruments and Ms. Kaori Iwazumi for the support of bacterial culture and the medium preparation.

Author contributions

R.K. and T.O. designed the study; R.K. conducted the experiment; R.K. analyzed the data; R.K. and T.O. wrote the paper.

References

1. L. J. Stal, R. Moezelaar, Fermentation in cyanobacteria *FEMS Microbiol. Rev.* **21**, 179–211 (1997).

2. T. Osanai, *et al.*, Genetic manipulation of a metabolic enzyme and a transcriptional regulator increasing succinate excretion from unicellular cyanobacterium *Front. Microbiol.* **6**, 1064 (2015).

3. H. Iijima, *et al.*, Four-carbon dicarboxylic acid production through the reductive branch of the open cyanobacterial tricarboxylic acid cycle in *Synechocystis* sp. PCC 6803. *Metab. Eng.* **65**, 88–98 (2021).

4. H. Iijima, *et al.*, Metabolomics-based analysis revealing the alteration of primary carbon metabolism by the genetic manipulation of a hydrogenase HoxH in *Synechocystis* sp. PCC 6803.

Algal Res. **18**, 305–313 (2016).

5. D. Carrieri, K. Wawrousek, C. Eckert, J. Yu, P.-C. Maness, The role of the bidirectional hydrogenase in cyanobacteria. *Bioresour. Technol.* **102**, 8368–8377 (2011).

6. V. Puggioni, S. Tempel, A. Latifi, Distribution of Hydrogenases in Cyanobacteria: A Phylum-Wide Genomic Survey. *Front. Genet.* **7**, 223 (2016).

7. C. Cassier-Chauvat, T. Veaudor, F. Chauvat, Advances in the function and regulation of hydrogenase in the cyanobacterium *Synechocystis* PCC6803. *Int. J. Mol. Sci.* **15**, 19938–19951 (2014).

8. K. Gutekunst, *et al.*, The bidirectional NiFe-hydrogenase in *Synechocystis* sp. PCC 6803 is reduced by flavodoxin and ferredoxin and is essential under mixotrophic, nitrate-limiting conditions. *J. Biol. Chem.* **289**, 1930–1937 (2014).

9. J. Appel, S. Phunpruch, K. Steinmüller, R. Schulz, The bidirectional hydrogenase of *Synechocystis* sp. PCC 6803 works as an electron valve during photosynthesis. *Arch. Microbiol.* **173**, 333–338 (2000).

10. J. H. Artz, *et al.*, The structure and reactivity of the HoxEFU complex from the cyanobacterium *Synechocystis* sp. PCC 6803. *J. Biol. Chem.* **295**, 9445–9454 (2020).

11. Y. Wang, *et al.*, Pyruvate:ferredoxin oxidoreductase and low abundant ferredoxins support aerobic photomixotrophic growth in cyanobacteria. *Elife* **11**, 2021.08.27.457892 (2022).

12. H. Burgstaller, *et al.*, *Synechocystis* sp. PCC 6803 Requires the Bidirectional Hydrogenase to Metabolize Glucose and Arginine Under Oxic Conditions. *Front. Microbiol.* **13**, 896190 (2022).

13. J. Hołówka, J. Zakrzewska-Czerwińska, Nucleoid Associated Proteins: The Small Organizers That Help to Cope With Stress. *Front. Microbiol.* **11**, 590 (2020).

14. A. Behle, *et al.*, Manipulation of topoisomerase expression inhibits cell division but not growth and reveals a distinctive promoter structure in *Synechocystis*. *Nucleic Acids Res.* **50**, 12790–12808 (2022).

15. T. C. Summerfield, S. Nagarajan, L. A. Sherman, Gene expression under low-oxygen conditions in the cyanobacterium *Synechocystis* sp. PCC 6803 demonstrates Hik31-dependent and -independent responses. *Microbiology* **157**, 301–312 (2011).

16. T. Osanai, *et al.*, Positive regulation of sugar catabolic pathways in the cyanobacterium *Synechocystis* sp. PCC 6803 by the group 2 sigma factor sigE. *J. Biol. Chem.* **280**, 30653–30659 (2005).

17. T. Osanai, *et al.*, Genetic engineering of group 2 sigma factor SigE widely activates expressions of sugar catabolic genes in *Synechocystis* species PCC 6803. *J. Biol. Chem.* **286**, 30962–30971 (2011).

18. J. Dutheil, *et al.*, The AbrB2 autorepressor, expressed from an atypical promoter, represses the hydrogenase operon to regulate hydrogen production in *Synechocystis* strain PCC6803. *J.*

496 *Bacteriol.* **194**, 5423–5433 (2012).

497 19. C. Leplat, *et al.*, Genome-wide transcriptome analysis of hydrogen production in the

498 cyanobacterium *Synechocystis*: Towards the identification of new players. *Int. J. Hydrogen*

499 *Energy* **38**, 1866–1872 (2013).

500 20. P. Oliveira, P. Lindblad, An AbrB-Like protein regulates the expression of the bidirectional

501 hydrogenase in *Synechocystis* sp. strain PCC 6803. *J. Bacteriol.* **190**, 1011–1019 (2008).

502 21. K. Gutekunst, *et al.*, LexA regulates the bidirectional hydrogenase in the cyanobacterium

503 *Synechocystis* sp. PCC 6803 as a transcription activator. *Mol. Microbiol.* **58**, 810–823 (2005).

504 22. P. Oliveira, P. Lindblad, LexA, a transcription regulator binding in the promoter region of the

505 bidirectional hydrogenase in the cyanobacterium *Synechocystis* sp. PCC 6803. *FEMS Microbiol.*

506 *Lett.* **251**, 59–66 (2005).

507 23. S. Imamura, M. Asayama, Sigma factors for cyanobacterial transcription. *Gene Regul. Syst. Bio.*

508 **3**, 65–87 (2009).

509 24. R. Kariyazono, T. Osanai, Identification of the genome-wide distribution of cyanobacterial group-

510 2 sigma factor SigE, accountable for its regulon. *Plant J.* **110**, 548–561 (2022).

511 25. A. Higo, E. Nishiyama, K. Nakamura, Y. Hihara, S. Ehira, cyAbrB Transcriptional Regulators as

512 Safety Devices To Inhibit Heterocyst Differentiation in Anabaena sp. Strain PCC 7120. *J.*

513 *Bacteriol.* **201** (2019).

514 26. A. Ishii, Y. Hihara, An AbrB-like transcriptional regulator, Sll0822, is essential for the activation
515 of nitrogen-regulated genes in *Synechocystis* sp. PCC 6803. *Plant Physiol.* **148**, 660–670 (2008).
516 27. J. Lieman-Hurwitz, *et al.*, A cyanobacterial AbrB-like protein affects the apparent photosynthetic
517 affinity for CO2 by modulating low-CO2-induced gene expression. *Environ. Microbiol.* **11**, 927–
518 936 (2009).
519 28. Y. Yamauchi, Y. Kaniya, Y. Kaneko, Y. Hihara, Physiological roles of the cyAbrB
520 transcriptional regulator pair Sll0822 and Sll0359 in *Synechocystis* sp. strain PCC 6803. *J.*
521 *Bacteriol.* **193**, 3702–3709 (2011).
522 29. K. Uyeda, J. C. Rabinowitz, Pyruvate-ferredoxin oxidoreductase. 3. Purification and properties of
523 the enzyme. *J. Biol. Chem.* **246**, 3111–3119 (1971).
524 30. P. M. Vignais, B. Billoud, Occurrence, classification, and biological function of hydrogenases: an
525 overview. *Chem. Rev.* **107**, 4206–4272 (2007).
526 31. M. Ortega-Ramos, *et al.*, Engineering *Synechocystis* PCC6803 for hydrogen production:
527 influence on the tolerance to oxidative and sugar stresses. *PLoS One* **9**, e89372 (2014).
528 32. N. Katayama, K. Iwazumi, H. Suzuki, T. Osanai, S. Ito, Malic Enzyme, not Malate
529 Dehydrogenase, Mainly Oxidizes Malate That Originates from the Tricarboxylic Acid Cycle in
530 Cyanobacteria. *MBio* **13**, e0218722 (2022).
531 33. T. Hasunuma, M. Matsuda, A. Kondo, Improved sugar-free succinate production by

532 *Synechocystis* sp. PCC 6803 following identification of the limiting steps in glycogen
533 catabolism. *Metab. Eng. Commun.* **3**, 130–141 (2016).
534 34. K. Song, *et al.*, Expression of the Cyanobacterial F(o)F(1) ATP Synthase Regulator AtpΘ
535 Depends on Small DNA-Binding Proteins and Differential mRNA Stability. *Microbiol. Spectr.*
536 **10**, e0256221 (2022).
537 35. D. Camsund, T. Heidorn, P. Lindblad, Design and analysis of LacI-repressed promoters and
538 DNA-looping in a cyanobacterium. *J. Biol. Eng.* **8**, 4 (2014).
539 36. T. Osanai, *et al.*, ChlH, the H subunit of the Mg-chelatase, is an anti-sigma factor for SigE in
540 *Synechocystis* sp. PCC 6803. *Proc. Natl. Acad. Sci. U. S. A.* **106**, 6860–6865 (2009).
541 37. H. Iijima, *et al.*, Changes in primary metabolism under light and dark conditions in response to
542 overproduction of a response regulator RpaA in the unicellular cyanobacterium *Synechocystis* sp.
543 PCC 6803 . *Front. Microbiol.* **6**, 888 (2015).
544 38. J. G. K. Williams, "Construction of Specific Mutations in Photosystem II Photosynthetic
545 Reaction Center by Genetic Engineering Methods in *Synechocystis* 6803" in *Methods in*
546 *Enzymology*, (Academic Press, 1988), pp. 766–778.
547 39. R. Rippka, J. Deruelles, J. B. Waterbury, Generic assignments, strain histories and properties of
548 pure cultures of cyanobacteria. *J. Gen. Microbiol.* **111**, 1–61 (1979).
549 40. S. Chen, Y. Zhou, Y. Chen, J. Gu, fastp: an ultra-fast all-in-one FASTQ preprocessor.

550 *Bioinformatics* **34**, i884–i890 (2018).

551 41. B. Langmead, S. L. Salzberg, Fast gapped-read alignment with Bowtie 2. *Nat. Methods* **9**, 357–

552 359 (2012).

553 42. S. Anders, P. T. Pyl, W. Huber, HTSeq--a Python framework to work with high-throughput

554 sequencing data. *Bioinformatics* **31**, 166–169 (2015).

555 43. M. D. Robinson, D. J. McCarthy, G. K. Smyth, edgeR: a Bioconductor package for differential

556 expression analysis of digital gene expression data. *Bioinformatics* **26**, 139–140 (2010).

557 44. Y. Zhang, *et al.*, Model-based analysis of ChIP-Seq (MACS). *Genome Biol.* **9**, R137 (2008).

558 45. M. Kopf, *et al.*, Comparative genome analysis of the closely related *Synechocystis* strains PCC

559 6714 and PCC 6803. *DNA Res.* **21**, 255–266 (2014).

560 46. A. R. Quinlan, I. M. Hall, BEDTools: a flexible suite of utilities for comparing genomic features.

561 *Bioinformatics* **26**, 841–842 (2010).

562 47. W. Shen, S. Le, Y. Li, F. Hu, SeqKit: A Cross-Platform and Ultrafast Toolkit for FASTA/Q File

563 Manipulation. *PLoS One* **11**, e0163962 (2016).

564 48. N. Takemata, R. Y. Samson, S. D. Bell, Physical and Functional Compartmentalization of

565 Archaeal Chromosomes. *Cell* **179**, 165-179.e18 (2019).

566 49. N. Takemata, S. D. Bell, Chromosome conformation capture assay combined with biotin

567 enrichment for hyperthermophilic archaea. *STAR Protoc.* **2**, 100576 (2021).

50. M. Abou El Hassan, R. Bremner, A rapid simple approach to quantify chromosome conformation capture. *Nucleic Acids Res.* **37**, e35 (2009).

51. , R: A Language and Environment for Statistical Computing (2022).

52. M. Hervé, RVAideMemoire: Testing and Plotting Procedures for Biostatistics (2022).

53. T. Wu, *et al.*, clusterProfiler 4.0: A universal enrichment tool for interpreting omics data. *Innov. (Cambridge* **2**, 100141 (2021).

575 **Table 1** List of transiently upregulated genes

		Operon
Oxidoreductase		
sll0741	*nifJ*/"pyruvate-ferredoxin/flavodoxin oxidoreductase"	TU3296
sll0743	hypothetical protein	
sll0744	dihydroorotate dehydrogenase (fumarate)	
sll1221	*hoxF*/“bidirectional [NiFe] hydrogenase diaphorase subunit”	TU1714
sll1222	unknown protein	
sll1223	*hoxU*/“bidirectional [NiFe] hydrogenase diaphorase subunit”	
sll1224	*hoxY*/“NAD-reducing hydrogenase small subunit”	
sll1225	unknown protein	
sll1226	*hoxH*/“NAD-reducing hydrogenase large subunit”	
slr1434	*pntB*/"H+-translocating NAD(P) transhydrogenase subunit beta"	TU1089
Transporter		
sll1450	*nrtA*/“nitrate/nitrite transport system substrate-binding protein”	TU1023
sll1451	*nrtB*/“nitrate/nitrite transport system permease protein”	
sll1452	*nrtC*/“nitrate/nitrite transport system ATP-binding protein”	
sll1453	*nrtD*/“nitrate/nitrite transport system ATP-binding protein”	
Two-component system		
slr1214	twitching motility two-component system response regulator PilG	TU905
slr1215	unknown protein	TU907
Glycosyl transferase		
slr2116	*spsA*/“spore coat polysaccharide biosynthesis protein; SpsA”	TU1673

Protease		
sll1009	*frpC*/"iron-regulated protein"	TU491
Insertion sequence (Transposase)		
slr1523	transposase	TU1659
sll1985	transposase	TU1589
sll7001	transposase	NA
sll7003	toxin FitB	TU7001
ssl0172	transposase	TU3163
Other		
slr1260	hypothetical protein	TU1446
slr0668	unknown protein	TU3532
slr5127	unknown protein	TU5127
sll0710	unknown protein	TU97
sll1307	unknown protein	TU1224

576 The list of transiently upregulated genes was merged by transcriptional units and sorted by function. The

577 transcriptional unit information was obtained from a previous study (Kopf et al., 2014).

578

579

580 **Figures and Figure legends**

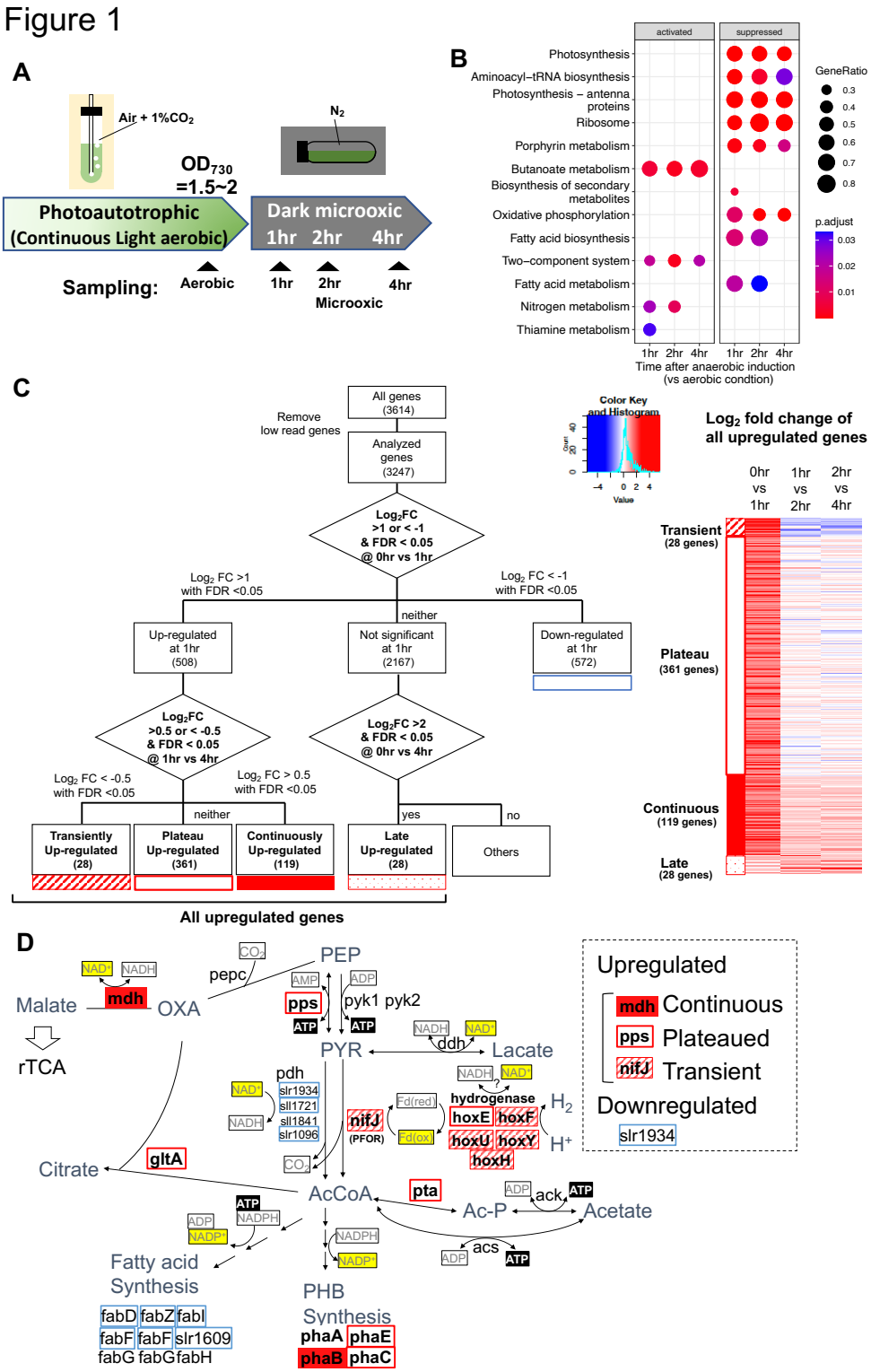

581

582 **Figure 1**

583 (A) Schematic diagram for the sampling of cells under aerobic and microoxic conditions. (B) Gene set
584 enrichment analysis on time-course transcriptome data. KEGG pathways enriched in upregulated or
585 downregulated genes after 1-, 2-, and 4-h incubation under microoxic conditions are shown. (C) (left)
586 Schematic diagram showing the classification of genes according to the time-course transcriptome.
587 Transient (striped square), Plateau (open square), Continuous (filled square), and Late (dotty square) are
588 denoted as all upregulated genes. (right) Heatmap showing expression change in all upregulated genes
589 over the time-course. Genes were clustered into subgroups and sorted by the gene name. (D) The
590 classified genes were mapped to the central carbon metabolism, centered on pyruvate. PEP:
591 phosphoenolpyruvate, PYR: pyruvate, AcCoA: acetyl CoA, Ac-P: acetyl phosphate, OXA: oxaloacetate,
592 PHB: polyhydroxy butyrate. rTCA: reverse tricarboxylic acid cycle.
593

Figure 2

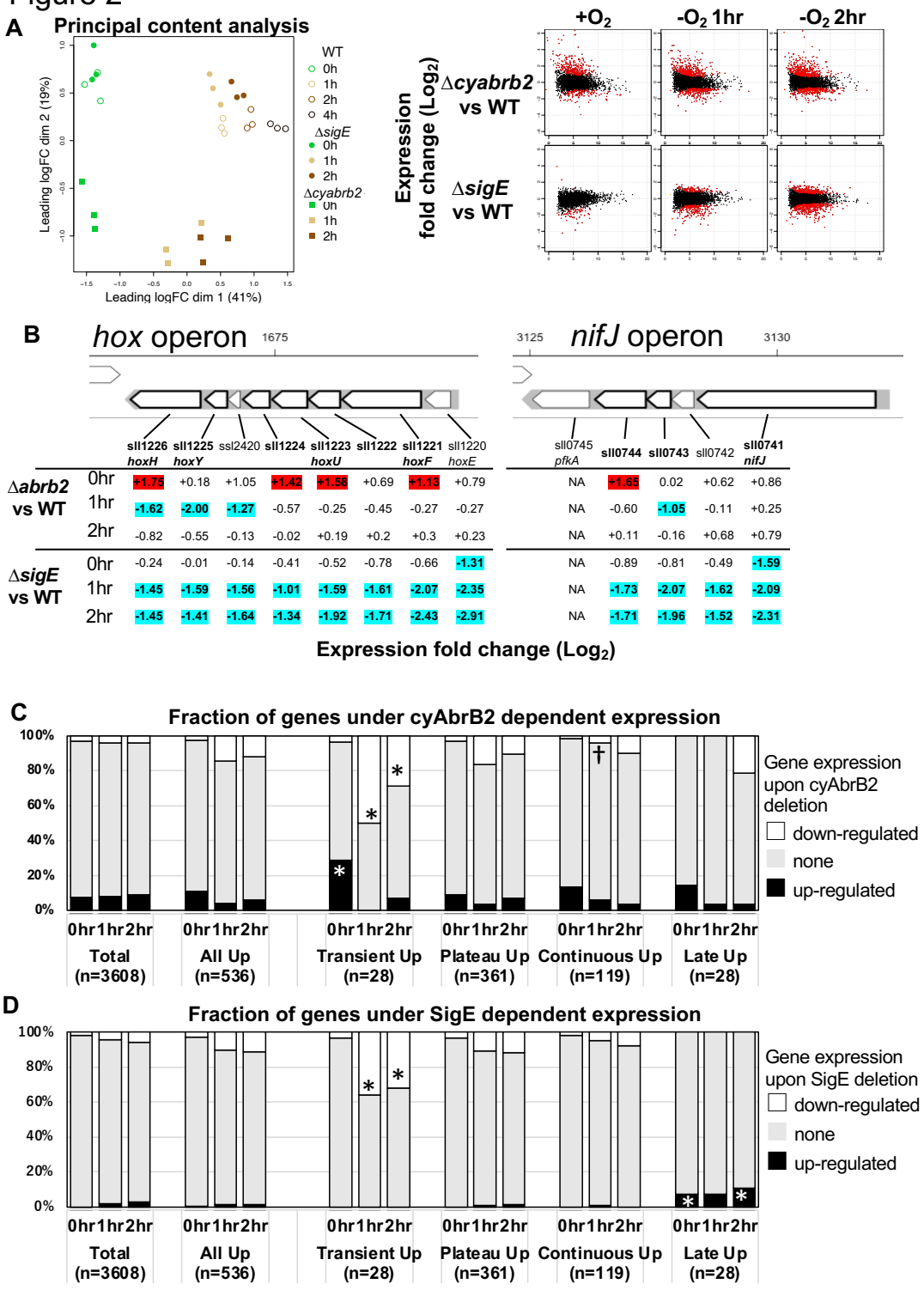

Figure 2

(A) (left) Primary component scatter plot showing the profiles of RNA-seq data. (right) MA plot showing

597 fold change (y-axis) and average (x-axis) of gene expression between wildtype and mutant strains at each

598 timepoint. Red dots indicate defined DEGs (|Log_2 FC| >1 with FDR < 0.05). (B) Log2 scaled expression

599 fold change in genes in the *hox* and *nifJ* operons upon Δ*cyabrb2* and Δ*sigE* under aerobic conditions (0

600 h), 1 hour after microoxic condition (1 hr), and 2 hours after microoxic condition (2 hr). DEGs are

601 marked with sky blue (downregulated upon deletion) or red (upregulated upon deletion). (C and D)

602 Fraction of upregulated and downregulated genes upon the (C) Δ*cyabrb2* and (D) Δ*sigE* at the timepoints

603 of aerobic conditions (0 hr), 1 hour after anoxic condition (1 hr), and 2 hour after anoxic condition (2 hr).

604 Genes are classified according to Figure 1C. Asterisk (*) and dagger (†) denote statistically significant

605 enrichment and anti-enrichment compared with all upregulated genes tested by multiple comparisons of

606 Fisher's exact test (FDR < 0.05).

607

Figure 3

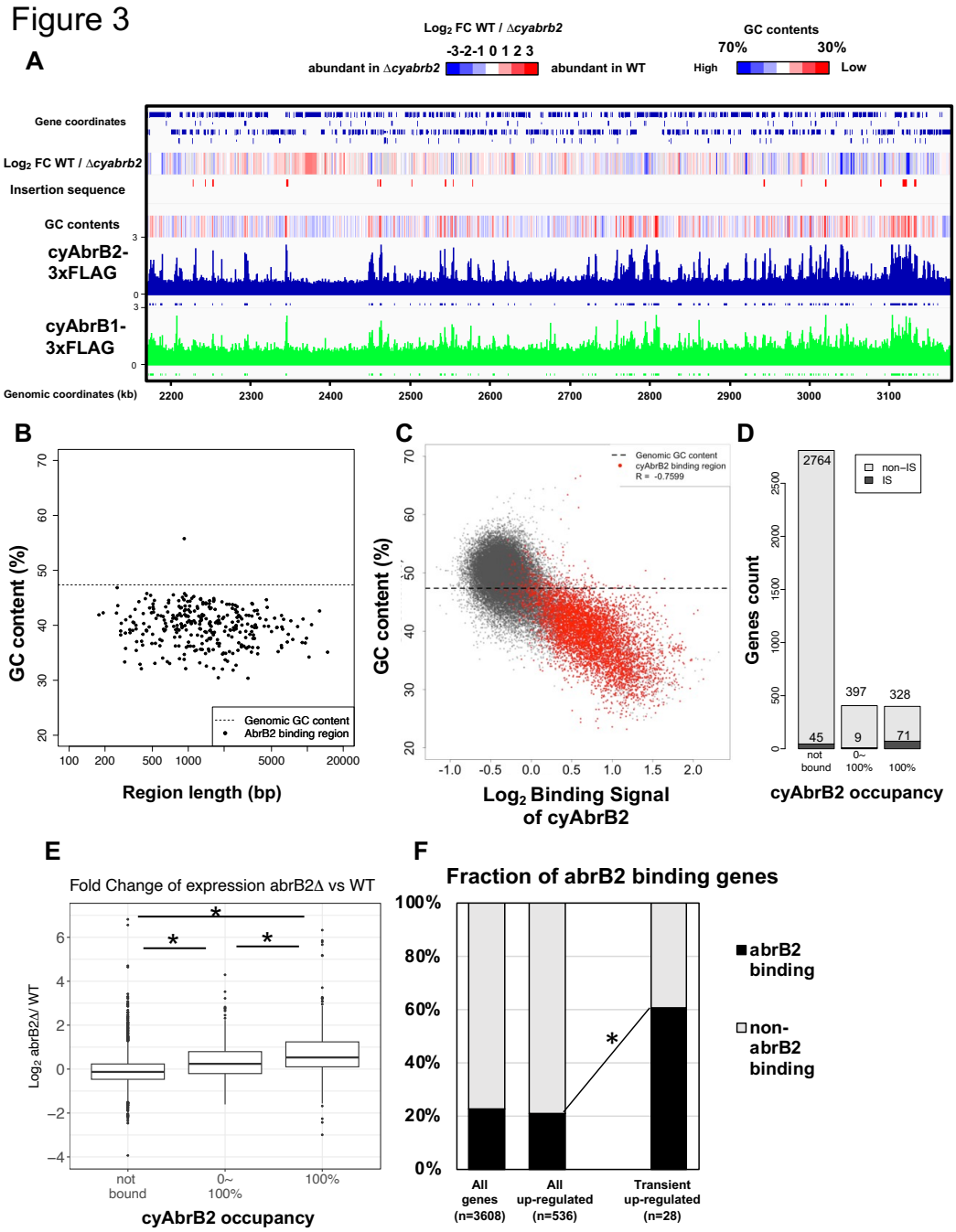

Figure 3 (continuing)

Figure 3 (continuing)

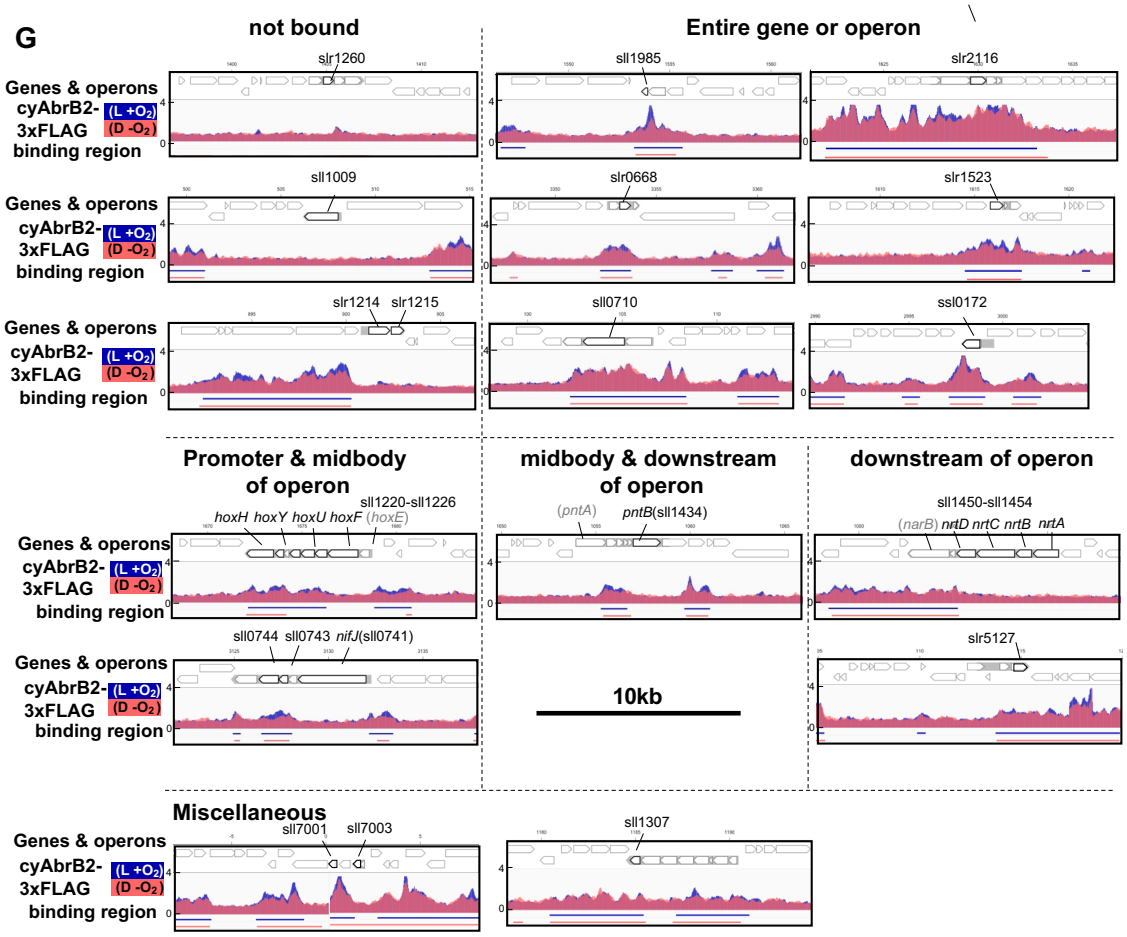

Figure 3

(A) Snapshot of ChIP-seq data for cyAbrB2 and cyAbrB1 under aerobic conditions. The heatmap in the second column indicates expression fold change upon Δ*cyabrb2* under aerobic conditions. Positive values (colored in red) indicate that the gene expression is higher in wildtype than in Δ*cyabrb2*, and negative values (colored in blue) indicate the opposite. The positions for the insertion elements are marked with red in the third column. The heatmap in the fourth column indicates GC contents. High GC content are colored in blue and low GC contents are colored in blue.

620 (B) GC contents and region length of cyAbrB2 binding regions (black dots). The horizontal dotted line

621 indicates the genomic average of GC content.

622 (C) Scatter plot of GC content and binding signal of cyAbrB2. The x-axis is the binding signal of

623 cyAbrB2 in each 100 bp region, and the y-axis indicates GC contents within 500 bp windows sliding

624 every 100 base pairs. CyAbrB2 binding regions are marked with red dots.

625 (D) Histogram of genes showing the extent of occupancy (not bound, partially overlapped, or entirely

626 overlapped) by the cyAbrB2 binding region. The gray bars indicate non-IS genes, and the count numbers

627 of the non-IS genes are displayed on the gray bars. The black bars indicate the IS genes, and the count

628 numbers of the IS genes are displayed above the black bars.

629 (E) Boxplot showing fold change in gene expression by Δ*cyabrb2* under aerobic conditions. Genes are

630 classified according to the extent of occupancy by the cyAbrB2 binding region. Asterisk (*) denotes

631 statistical significance tested by multiple comparisons of the Wilcoxon-rank test.

632 (F) Fraction of genes overlapped or non-overlapped with cyAbrB2 binding regions at the timepoints of

633 aerobic conditions. Genes are classified according to Figure 1C. Asterisk (*) denotes statistically

634 significant enrichment compared with all upregulated genes tested by multiple comparisons of Fisher's

635 exact test.

636 (G) Distribution of cyAbrB2 around transiently upregulated genes. ChIP-seq data in aerobic (L + O_2) and

637 dark microoxic (D − O_2) conditions are overlayed. Arrows with bold lines indicate transiently upregulated

genes. Shaded arrows indicate operons whose data were obtained from a previous study. The bars below the graph indicate the binding regions of each protein. The black bar at the top of the figure indicates a length of 10 kbp.

Figure 4

A

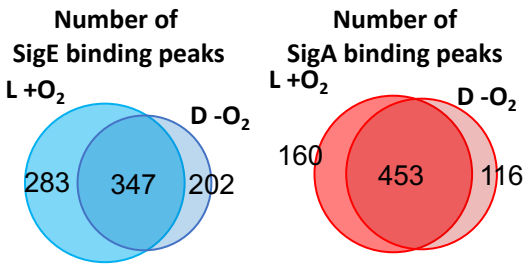

C

		no SigE summit	SigE summit
cyAbrB2	free	1071	598
	bound	280	32
Odds ratio	0.205	p-value	< 2.2e-16

		no SigA summit	SigA summit
cyAbrB2	free	1105	564
	bound	263	49
Odds ratio	0.365	p-value	3.95e-11

B

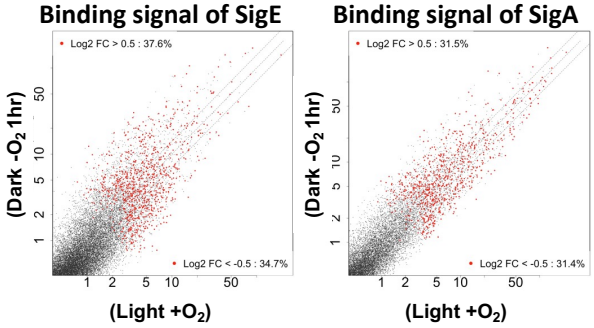

D

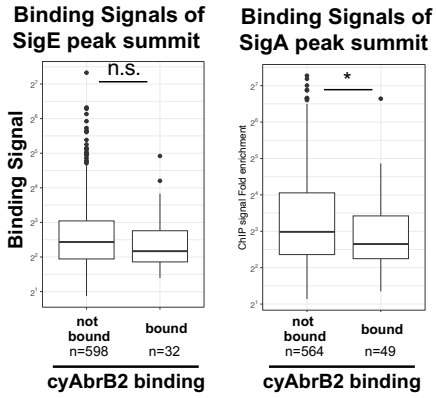

E

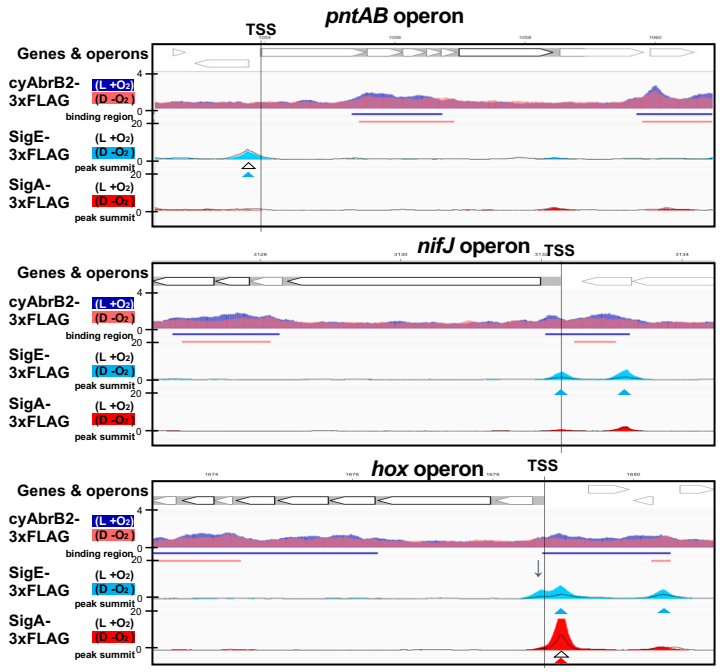

Figure 4

(A) Venn diagram showing the number of peaks of SigE (left) and SigA (right) in aerobic (L + O_2) and

645 dark microoxic (D − O_2) conditions. (B) Scatter plot showing changes in the binding signal of SigE and

646 SigA by 1 hour cultivation under microoxic conditions. The binding signal of each 100 bp window is

647 plotted. The binding signals are plotted in Figure 3E. (C) 2x2 tables showing co-occurrence of cyAbrB2

648 bindingregions and SigE peaks (top) or SigA binding peaks (bottom). Odds and p-values were calculated

649 by Fisher's exact test. (D) Distribution of ChIP enrichment signals of SigE and SigA peaks. The peaks

650 were classified into two based on whether they overlapped with the cyAbrB2-binding region. (E)

651 Snapshots of ChIP-seq data for CyAabrB2, SigE, and SigA at the *nifJ* region (top) and *hox* region

652 (bottom). ChIP-seq data for cyAbrB2, SigE, and SigA under aerobic and dark microoxic conditions are

653 overlayed. ChIP-seq data of cyAbrB2 under aerobic and microoxic conditions are colored blue and pink,

654 respectively. ChIP-seq data for SigE and SigA are shown in solid lines (aerobic conditions) and filled

655 lines (microoxic conditions). The positions of TSSs were obtained from a previous study (Kopf et al.,

656 2014) and indicated by vertical dotted lines. Open triangles indicate peak summits under aerobic

657 conditions, and solid triangles indicate peak summits under microoxic conditions.

Figure 5

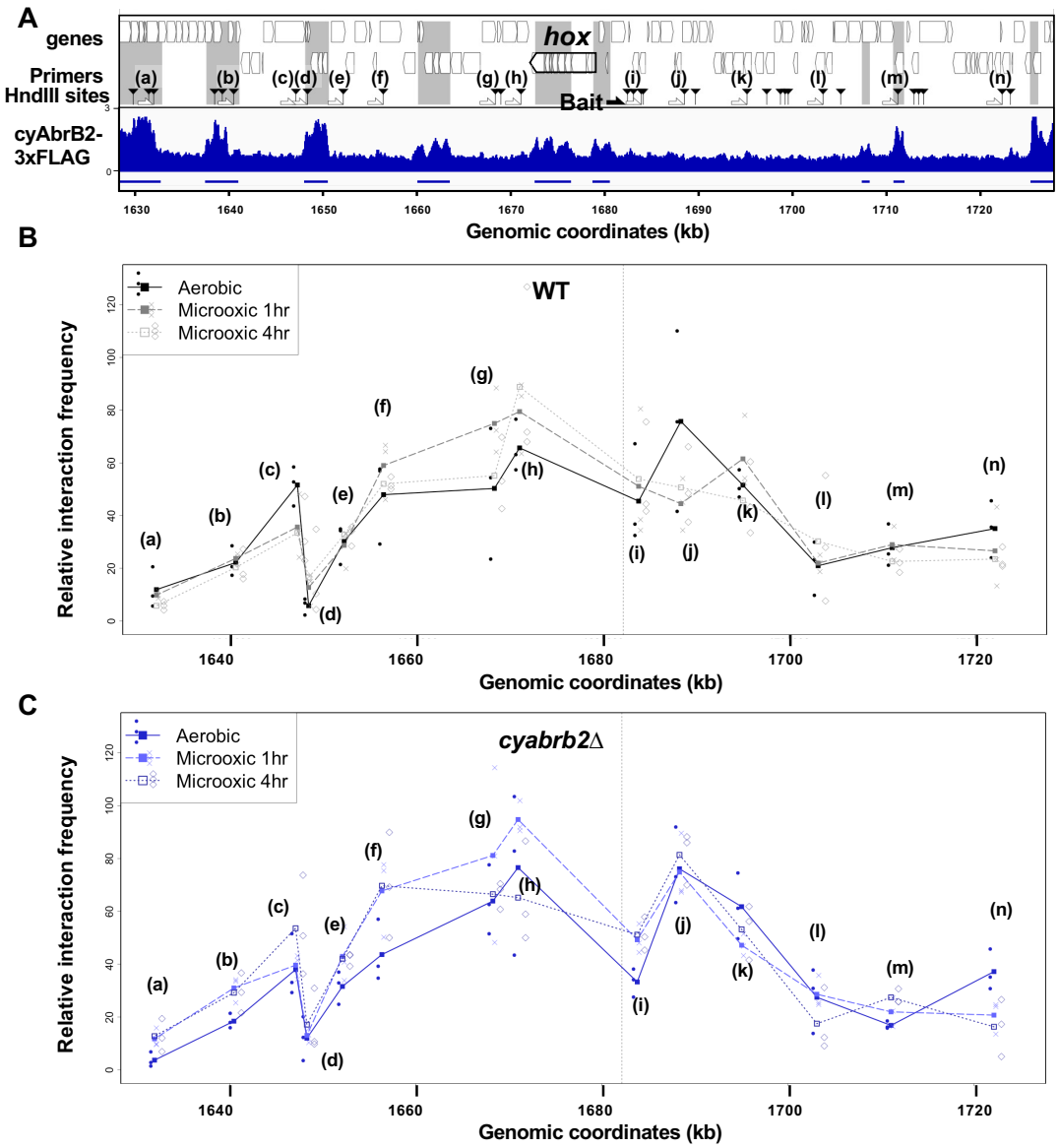

Figure 5 (continuing)

Figure 5 (continued)

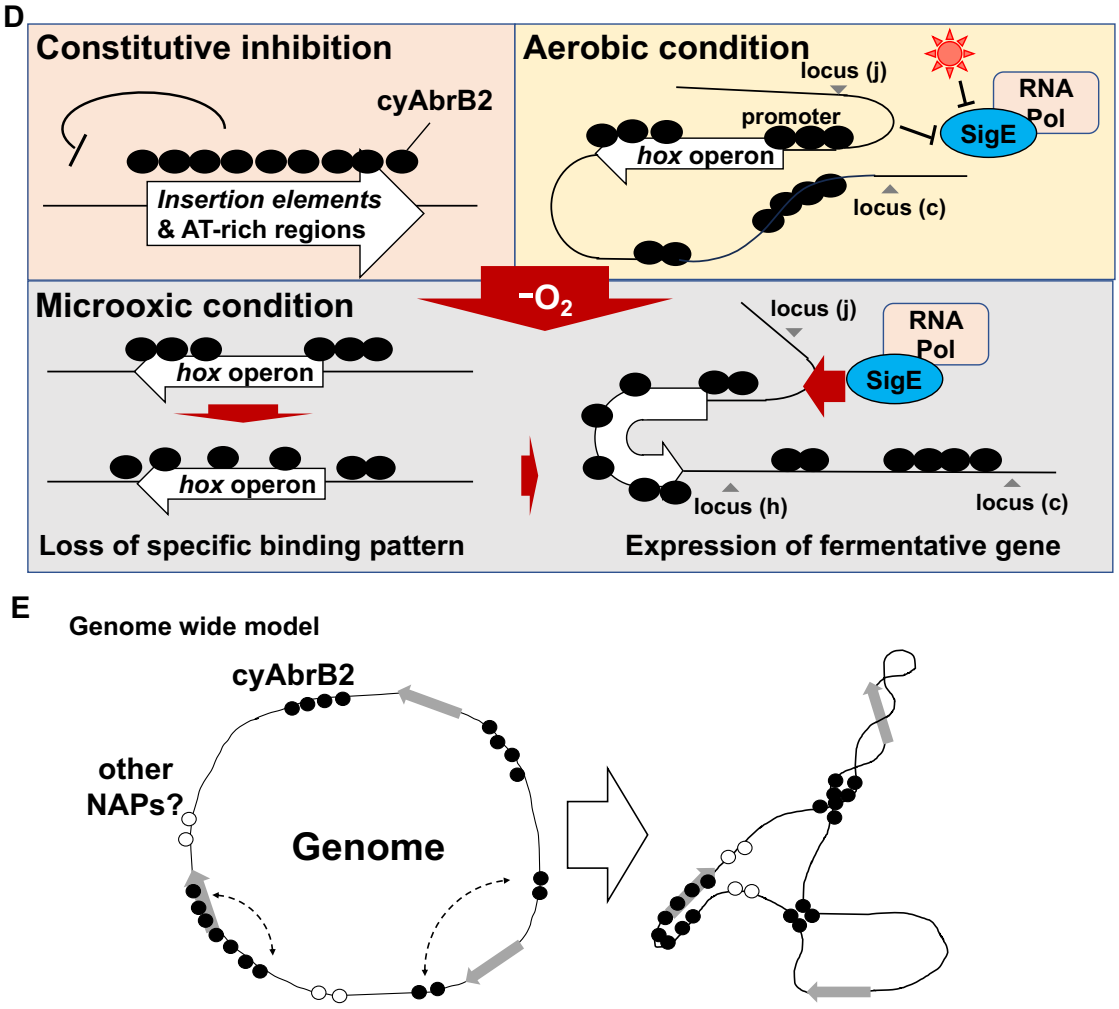

Figure 5

(A) Schematic diagram of 3C analysis around *hox* operon. The black arrow shows the localiton of the bait primer, and white arrows ((a) to (n)) indicate loci where the interaction frequency with bait were assayed. Black arrowheads indicate the position of HindIII sites. ChIP-seq data of cyAbrB2 in the aerobic condition is displayed in the bottom, and cyAbrB2 binding regions are marked with shade. (B) and (C) The line plot showing the interaction frequency of each locus with *hox* fragment in the wildtype (B) and Δ*cyabrb2* (C). The solid, dashed, and dotty lines indicate data in the aerobic condition, 1hr, and 4hr

672 cultivation of microoxic conditions, respectively. The line plots indicate the average interaction frequency

673 over the random ligation (n=3). Indivisual data are plotted as dots. (D) Schematic diagram of the

674 dynamics of transcription factors governing fermentative gene expression. (E) The model showing

675 cyAbrB2 shapes higher order DNA structure of the cyanobacterial chromosome.

676

Figure S1

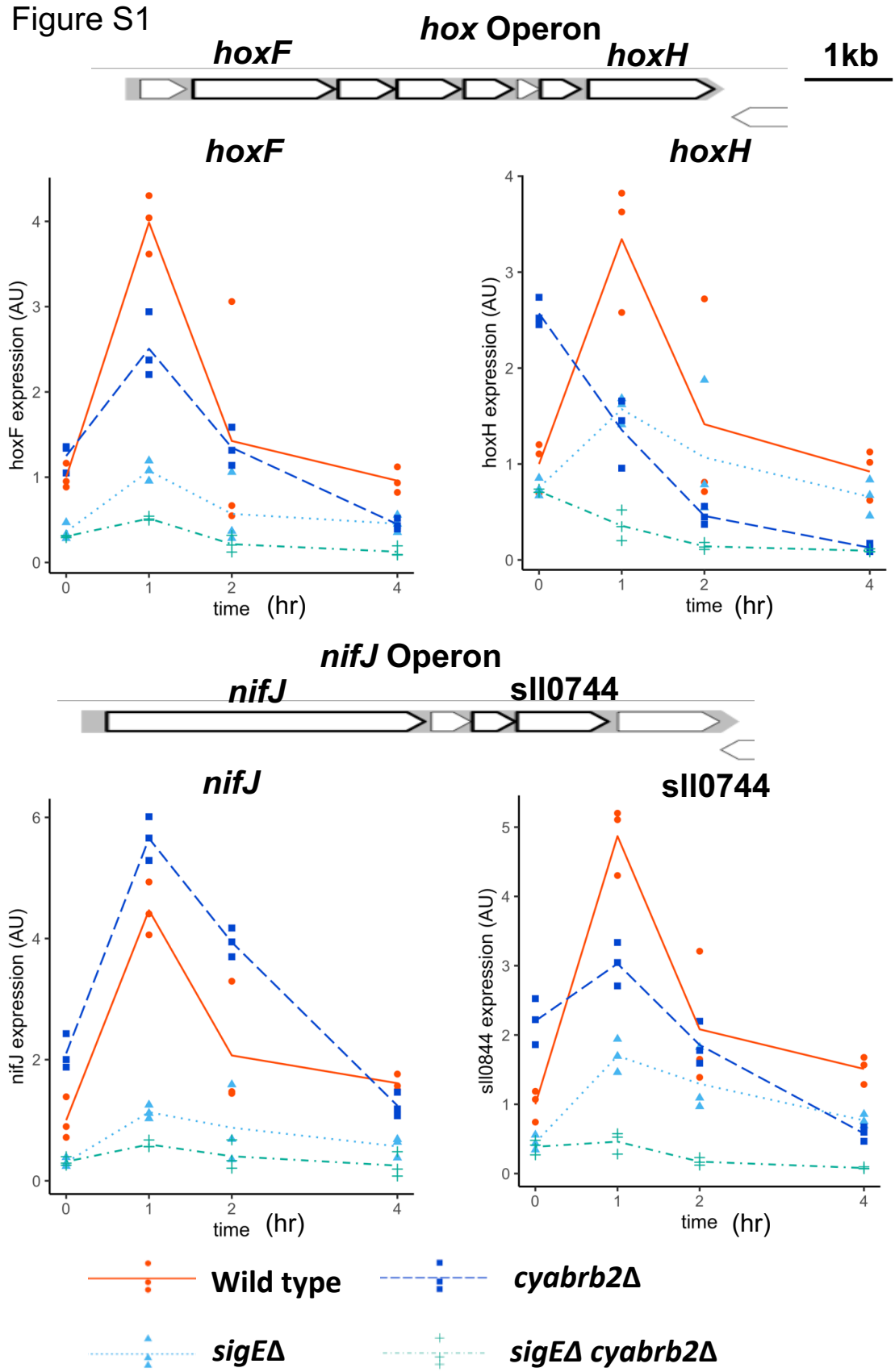

677

678 **Figure S1**

679 RT-qPCR validated the transiently upregulated genes classified by RNAseq. Transcripts extracted from

680 wildtype (solid line), Δ*sigE* mutant (dotty line), Δ*cyabrb2* mutant (dashed line), and Δ*sigE* Δ*cyabrb2*

681 double mutant (dot-dashed line) were assayed in the aerobic condition (0hr) and 1,2,4 hour incubation of

682 microoxic conditions. As the representative of the transiently upregulated genes, expression of *hoxF*,

683 *hoxY, nifJ,* and *sll0744* were quantified by RT-qPCR. The line represents the mean of n=3, and individual

684 data points are shown as dot plots. Data of each gene is normalized by the mean score of wildtypes in the

685 aerobic condition.

Figure S2

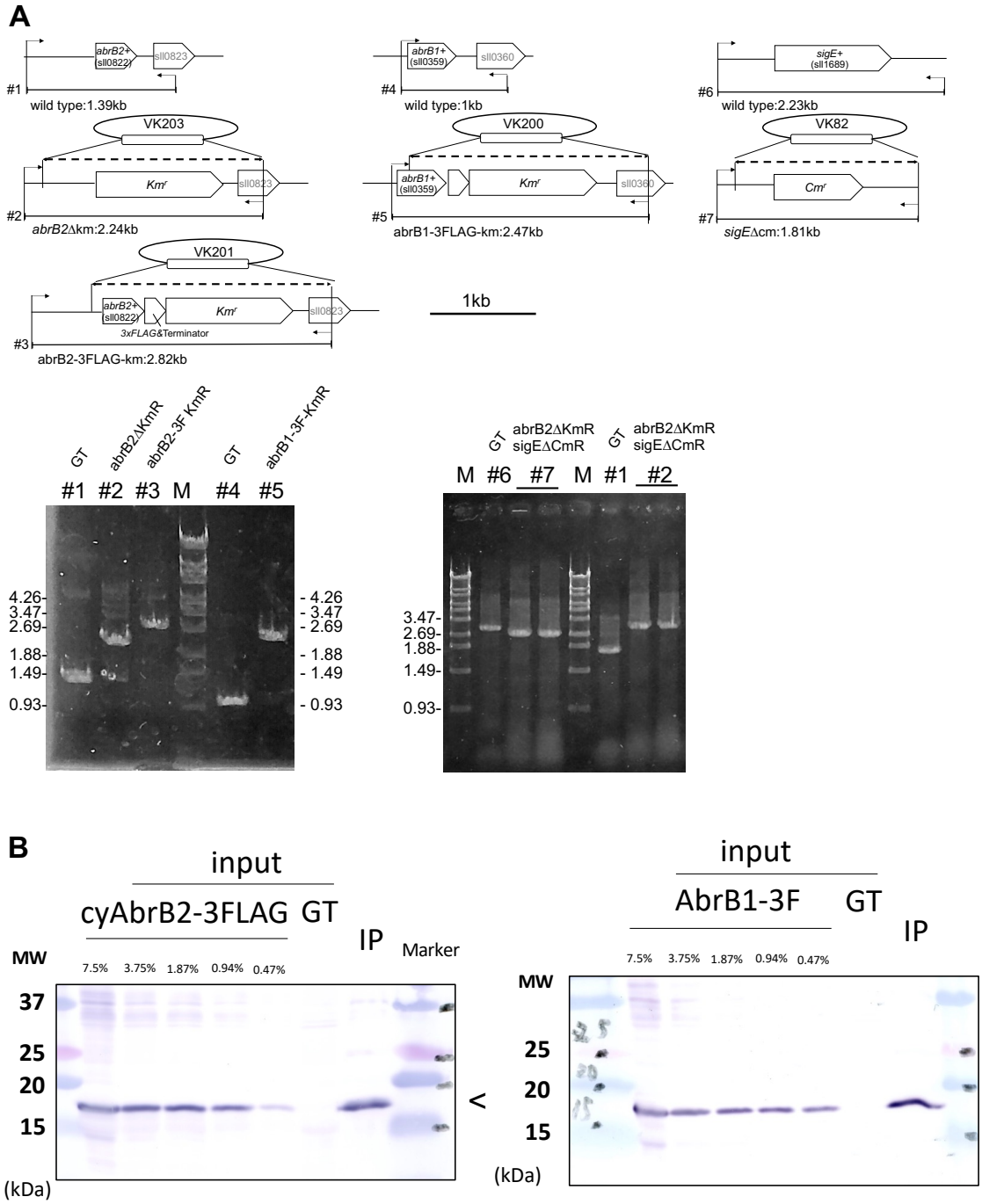

686

687 Figure S2 (continuing)

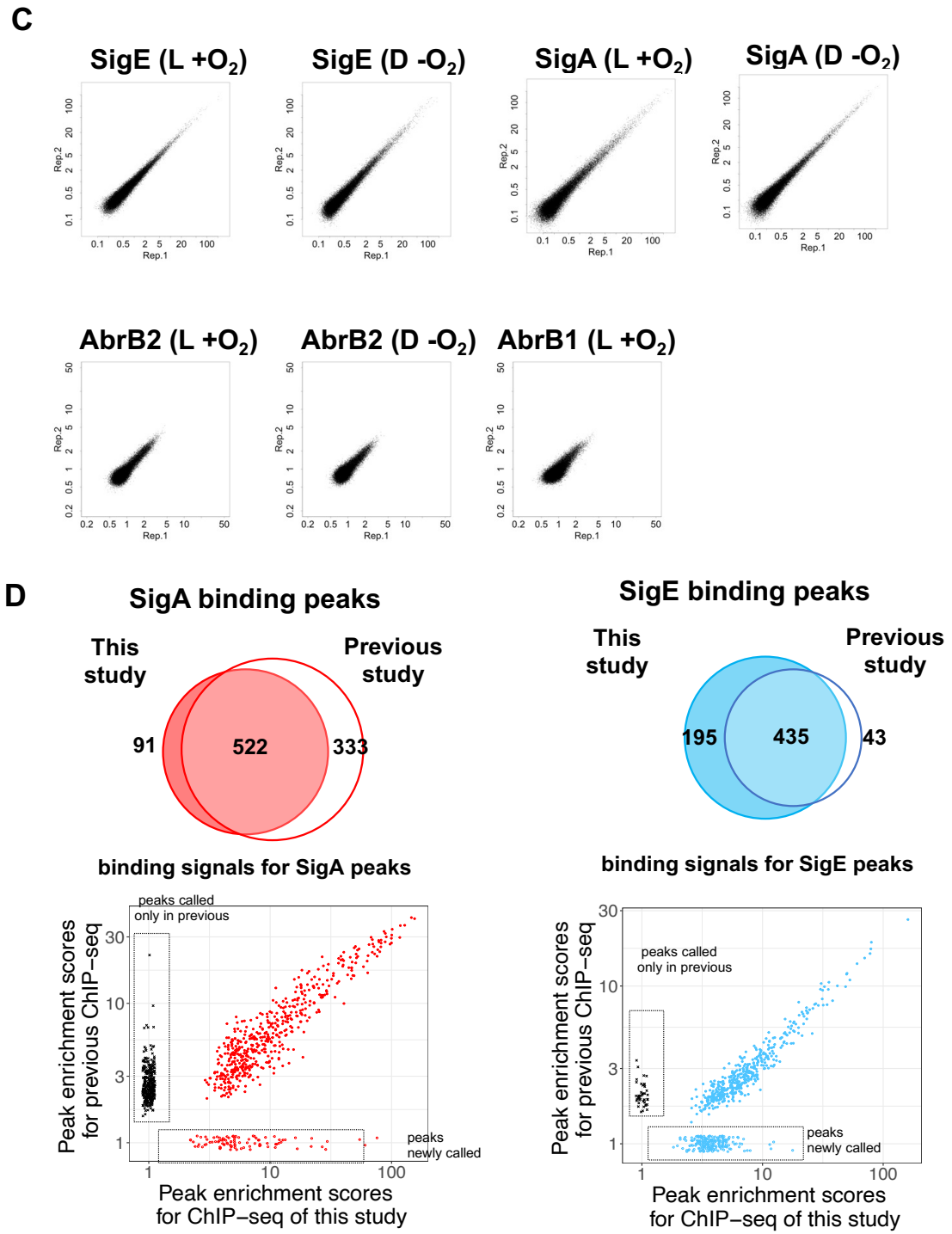

Figure S2 Genotyping and the procedure for ChIP-seq of flag-tagged proteins

Validation of procedure for ChIP-seq of flag-tagged cyAbrB2, SigE, and SigA.

(A) Confirmation of genomic deletion and the epitope tagging of *abrB2* (#1-#3), the epitope tagging of

692 *abrB1* (#4 and #5), and deletion of *sigE* (#6 and #7). Dotty lines are homologous regions between

693 plasmids and the genome. Arrows indicate position of check primers. (B) The immunoblot for inputs and

694 immunoprecipitants of ChIP for cyAbrB2-FLAG and cyAbrB1-FLAG. Inputs equivalent to the indicated

695 portion of IP were loaded. (C)Scatter plots showing the reproducibility of two replicates for ChIP-seq

696 assay. ChIP-seq data of SigE, SigA, and cyAbrB2 in aerobic and microoxic conditions and ChIP-seq data

697 of cyAbrB1 in the aerobic condition are shown. Dots indicate normalized IP read count / normalized input

698 read count in each 100bp window. X-axis is the value of replicate1, and Y-axis is the value of replicate 2.

699 (D) Reproducibility of ChIP-seq data of SigA and SigE, compared with the previous study (Kariyazono

700 and Osanai 2022). (top) Pie charts show the overlapping of peaks called in this study and the previous

701 study. (bottom) Scatter plot comparing ChIP binding signals of SigA and SigE peaks commonly called in

702 present and previous studies. Plots boxed by dashed lines are peaks called only in the present or previous

703 study.

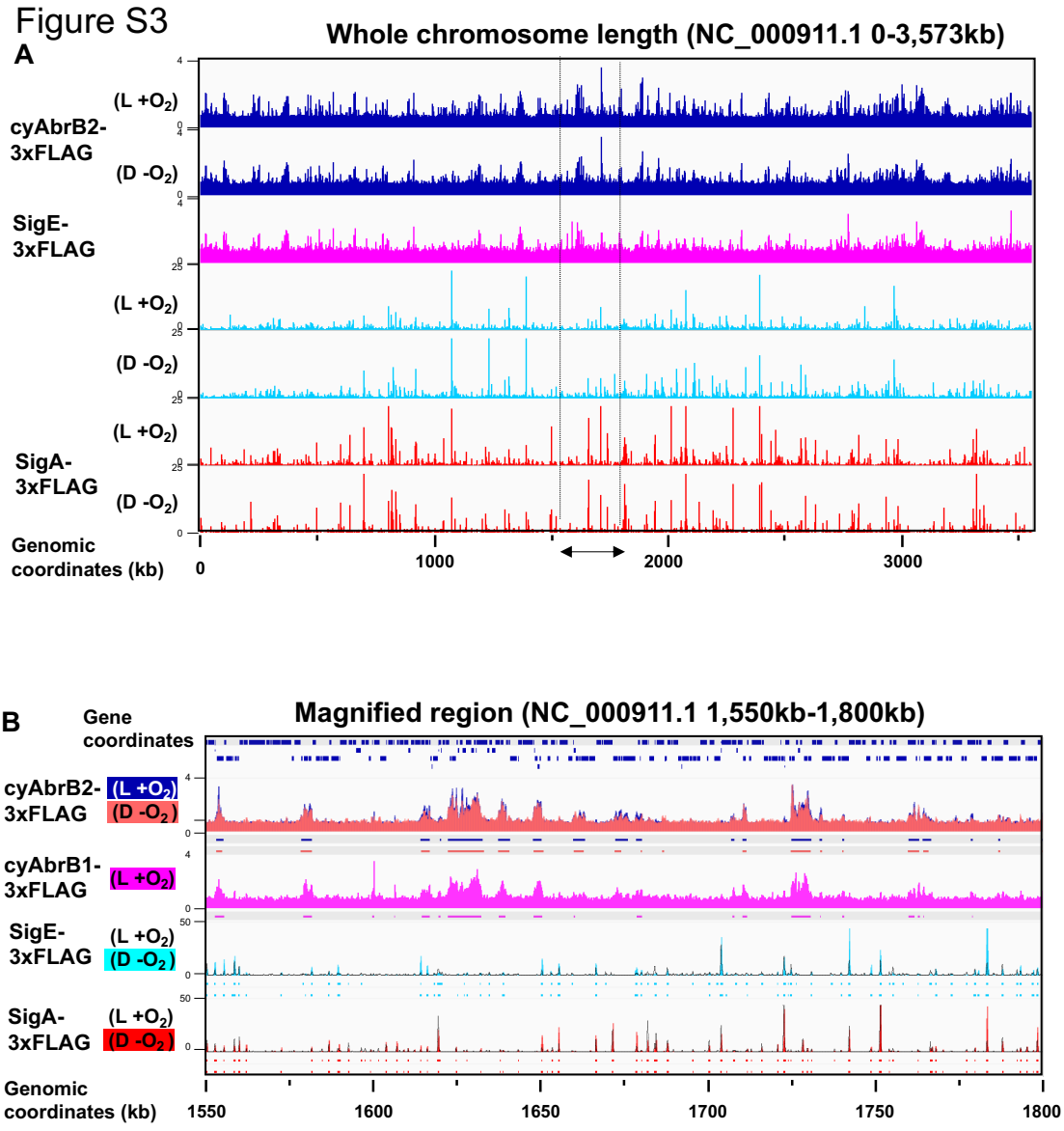

Figure S3 Overview of ChIP-seq data

Overview for ChIp-seq of flag tagged cyAbrB2, cyAbrB1, SigE, and SigA. Y-axis indicates [normalized IP read count / normalized input read count at each 25bp window], and X-axis indicates chromosome position.

(A) Distribution of cyAbrB2, cyAbrB1, SigE, and SigA across the whole genome of *Synechocystis*. Aerobic (L +O_2) and dark microoxic (D -O_2) data are displayed. (B) Magnified image for chromosome

711 position of 1,550kb-1,800kb. ChIP-seq data of cyAbrB2, cyAbrB1, SigE, and SigA in aerobic and dark

712 microoxic conditions are overlayed. The dots below the graph indicate the binding region of each protein

713 calculated by peak caller.

714

Figure S4

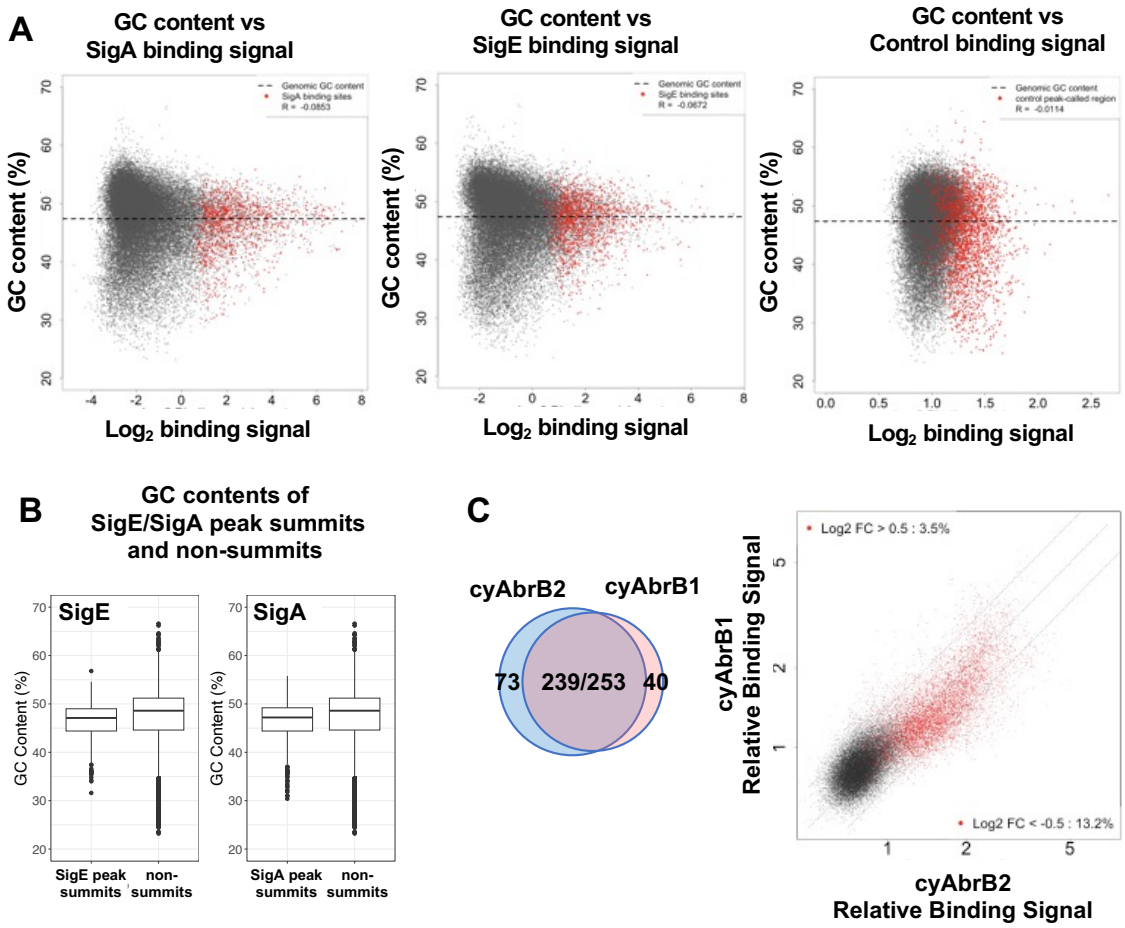

Figure S4 GC content vs ChIP enrichment score of SigA and SigE

(A) Scatter plot showing GC contents in each 100bp vs. binding signal of SigA, SigE, and control IP. Data are displayed as in Figure 3C. (B) GC content in each 100bp of (left) SigE peaks and non-SigE peaks, and (right) SigA peaks and non-SigA peaks. (C) Venn diagram showing overlap of the binding region of cyAbrB1 and cyAbrB2 (left), and scatter plot showing ChIP binding signal of cyAbrB2 (y-axis) and cyAbrB1(x-axis) in the aerobic condition. Data is plotted as in Figure 4E.

Figure S5

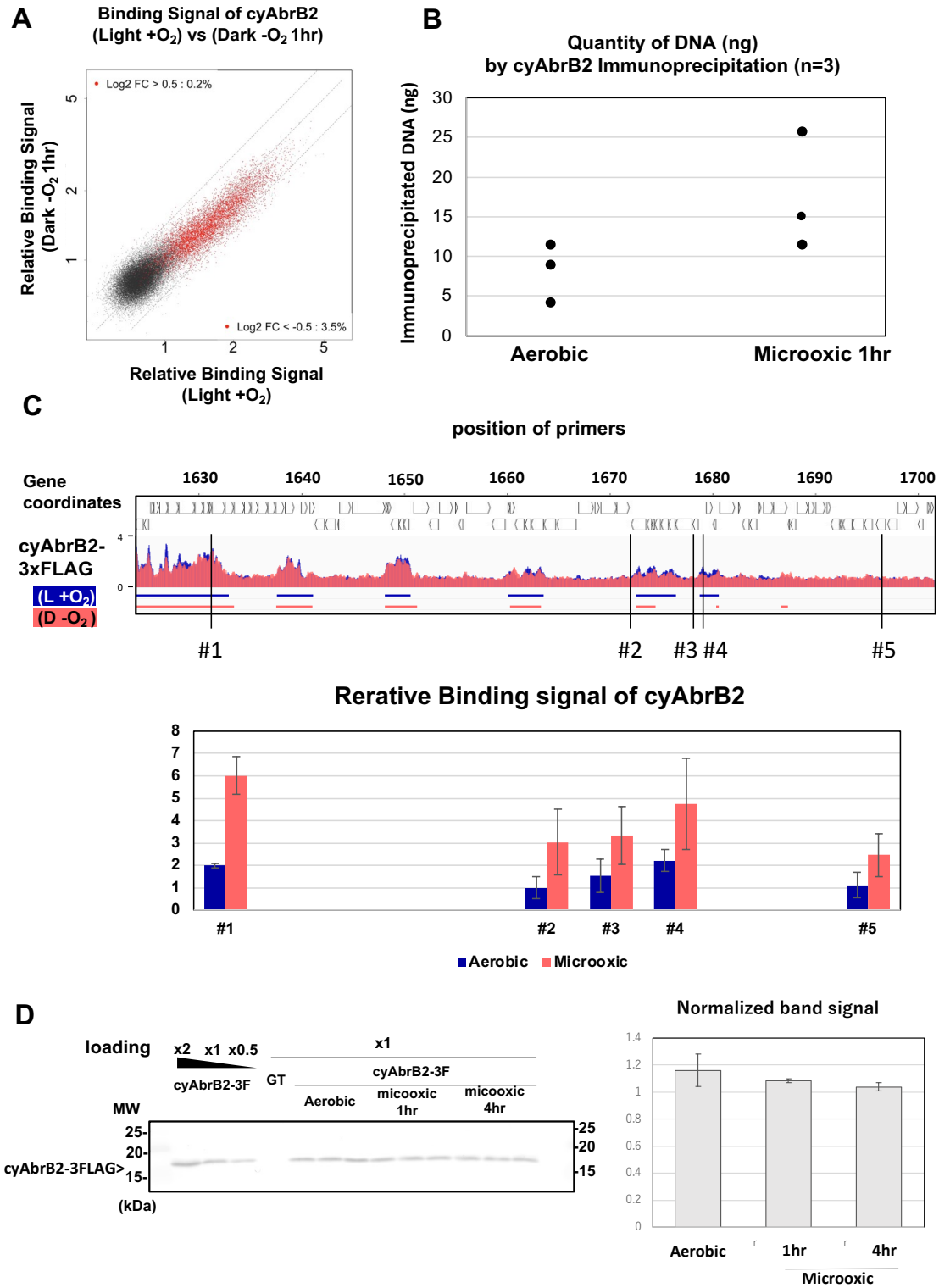

723

724

725 **Figure S5 Alteration of cyAbrB2 binding to genome under the microoxic condition**

726 (A) Scatter plot showing changes of the binding signal by 1hr cultivation in the microoxic condition. The
727 binding signal of each 100bp window is plotted. Red dots are cyAbrB2 binding regions in either aerobic
728 or microoxic conditions. The dotty lines indicate Log2 fold enrichment of 0.5, 0, -0.5 between aerobic
729 and microoxic conditions. (B) Amount of precipitated DNA by cyAbrB2 ChIP. Three experiments were
730 performed in the aerobic and microoxic conditions. (C) Quantification for ChIP of cyAbrB2 by qPCR.
731 The position of primers and ChIP-seq data of cyAbrB2 are shown at the top. (D) Western blot images of
732 cyAbrB2-3FLAG. Proteins were extracted in the aerobic condition and 1hr and 4hr incubation under
733 microoxic conditions. The total protein concentration of each sample was adjusted to 4mg/mL, measured
734 by the BCA method. Quantification of cyAbrB2 from western blot image was performed by ImageJ (ver.
735 2.0.0-rc-65) and plotted in the right graph.

736

Figure S6

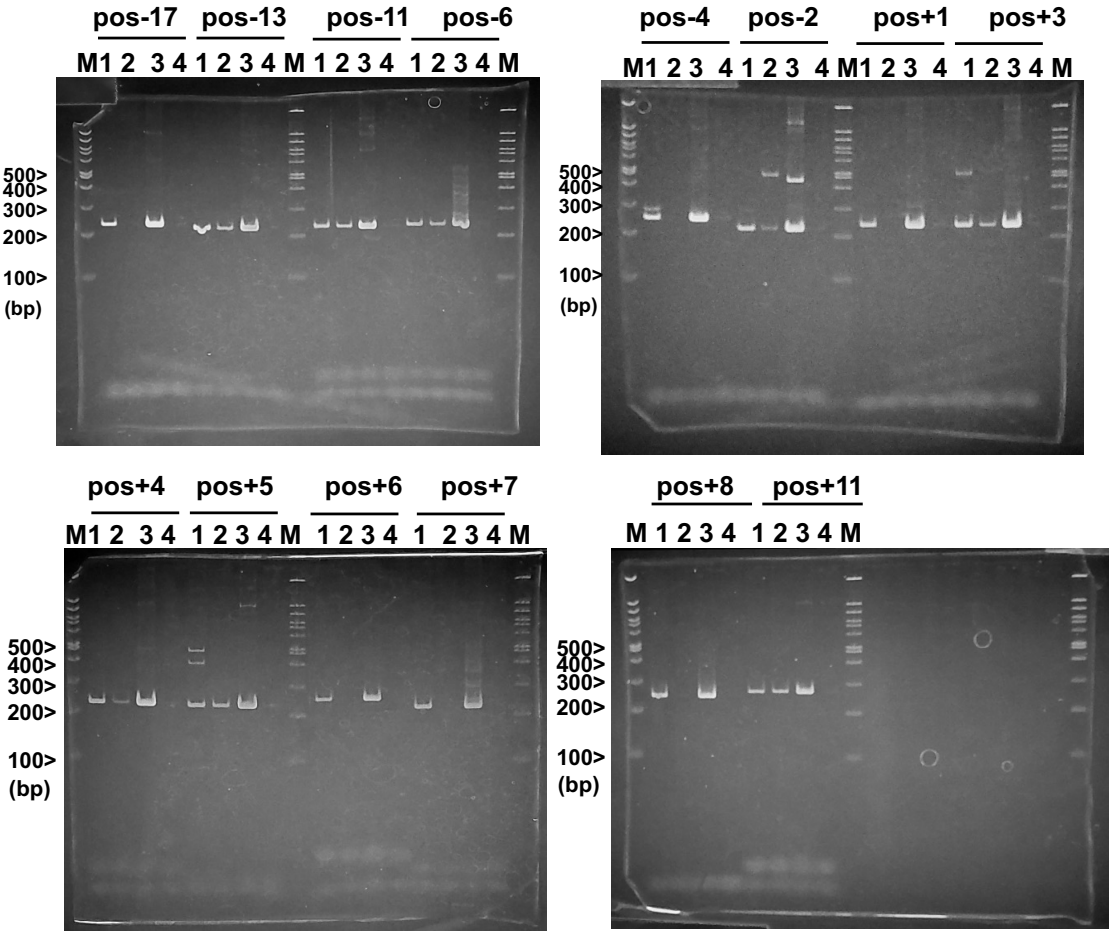

M:100bp ladder (DM2100 SMOBIO)
1 Calibration sample x500
2 Calibration sample x2500
3 3C sample x100
4 Unligated sample x100

GoTaq® Hot Start Program

95˚C 2min
95˚C 15sec | **x35**
60˚C 30sec
4˚C Hold

Figure S6 Validation of unidirectional primer sets for 3C assay

The validation of unidirectional primer sets for 3C assay is shown in Figure 5. The 3C sample in this assay is the mixture of all 3C samples assayed in Figure 5.

Figure S7

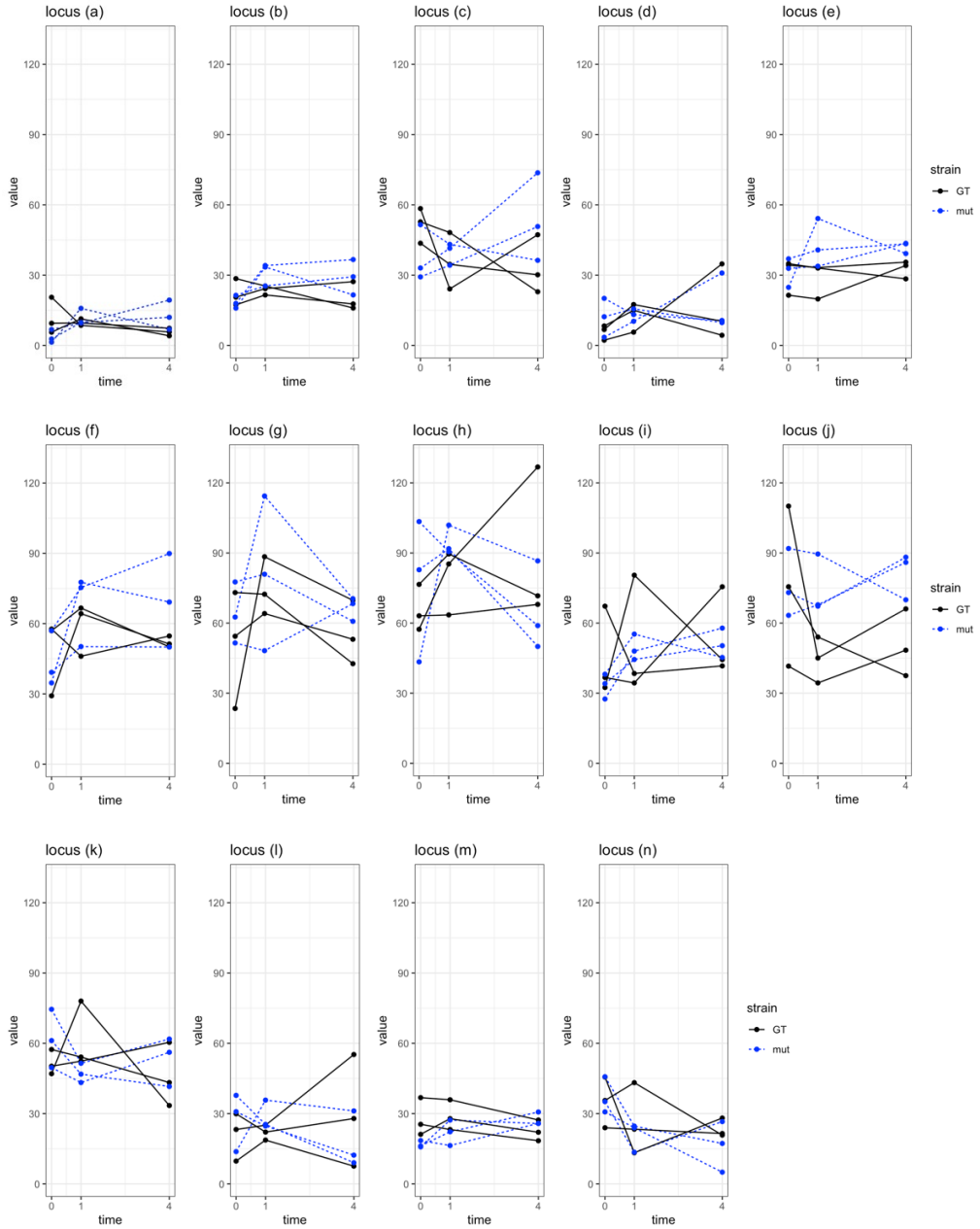

741

742 **Figure S7 Dynamics of individual 3C scores**

743 Re-plotting of Figure 5B and 5C with the x-axis showing time (0,1,4 hr in microoxic conditions) and the

744 y-axis showing the interaction frequency. Plots from the individual samples are connected by solid

745 (Wildtype) or dotty (Δ*cyabrb2*) lines.

746 **Table S1 Fold changes of transcripts from *sigA, sigB, sigC, sigD, and sigE***

		0hr vs 1hr		1hr vs 4hr	
Sigma factor	**locus**	**Log2FC**	**FDR**	**Log2FC**	**FDR**
SigA	slr0653	-0.873248	0.00766486	-0.0013514	0.99797563
SigB	sll0306	1.38098826	8.42E-06	0.77453605	0.04057775
SigC	sll0184	2.97101055	1.75E-16	1.30743549	0.00067892
SigD	sll2012	0.4701823	0.1498473	-0.4522181	0.32402556
SigE	sll1689	-1.9111759	1.96E-11	-1.1223298	0.00633142

747 Data is extracted from Supplemental Table S7.

748

749 **Table S2 List of strains used in this study**

Strain ID	**Host strain**	**genotype**	**Reference**
GT			Williams, 1988
G50	GT	Δ*sigE::*KmR	T. Osanai, et al,2005
KR93	GT	SigA-8His-KmR	(Kariyazono and Osanai 2022)
KR94	GT	SigA-3FLAG-KmR	(Kariyazono and Osanai 2022)
KR340	GT	Δ*cyabrb2::*KmR	in this study
KR338	GT	cyAbrB(sll0359)-3xFLAG-KmR	in this study
KR339	GT	cyAbrB2(sll0822)-3xFLAG-KmR	in this study
KR359	KR340	Δ*cyabrB2::*KmR Δ*sigE::*CmR	in this study

750

751 **Table S3 plasmids used in this study**

Plasmid ID		**backbone**	
VK82	*sigE*ΔCmR	pTA2 (Toyobo)	transformation for KR359
VK200	AbrB1-3F-KmR	pTA2 (Toyobo)	transformation for KR338

VK201	AbrB2-3F-KmR	pTA2 (Toyobo)	transformation for KR339
VK203	*cyabrB2*ΔKmR	pTA2 (Toyobo)	transformation for KR340

752

753 **Table S4 oligonucleotides used in this study**

Oligonucleotides ID		**sequence**
qPCR_hoxF_F	Figure S1	GTCATCTGCAATGCTGACGAA
qPCR_hoxF_R	Figure S1	CCAACACACTGCGGTCCAT
qPCR_hoxH_F	Figure S1	TCCCGTTACCCGGATTGA
qPCR_hoxH_R	Figure S1	GCCCTGGTCGTTGAGGAAA
qPCR_nifJ_sll0741_F	Figure S1	GATTCGGGGCAAAGTTTACG
qPCR_nifJ_sll0741_R	Figure S1	TACCTGGATGGTGAACTTAG
qPCR_sll0744_F	Figure S1	GCAGCTTAAATGGTTCTACC
qPCR_sll0744_R	Figure S1	CCAAATCTGTGGGTACGTAG
qPCR_nrpB_F	Figure S1	AAAGGGTAAGGGTGCAAAGG
qPCR_nrpB_R	Figure S1	AATTCCTCAAGCGGTTCCAC
new_abrB_0822_del_chkF	Figure S2A	AATCCTCCGCCAAACTTTG
abrB_0822_tag4	Figure S2A	GGAGTTTTCACCATCAGTC
abrB_0359_chkF	Figure S2A	AGAGGGAAAAATTCCTCGGC
abrB_0359_tag4	Figure S2A	TCGCCAGGGAAAGTAATTGG
SigE_whole_del_chkF	Figure S2A	GGAACGCTTGGAATGGCAAC
sigE_tag4	Figure S2A	TGAAGGGGGTAGATTTAAGCC
ChIP_slr2118_F1	Figure S5C #1	CATTTCAAGCGAGATAGCAG
ChIP_slr2118_R1	Figure S5C #2	TGGAAAGTGCCTGTTCAAAG
ChIP_ThoxH_F	Figure S5C #2	CATCACCGAGGGCATATCTAG
ChIP_ThoxH_R	Figure S5C #2	ACATAAGGCTATGGAAACC
ChIP_pHox_2F	Figure S5C #3	ACAGAGGATGGACAAATGTC
ChIP_pHox_2R	Figure S5C #3	TACCGCTTCGTCATTCTGCT
ChIP_pHox_up_2R	Figure S5C #4	TCGATTACTTCCCTTTAGTG
ChIP_pHox_up_2F	Figure S5C #4	CTTCGGCTCCATGTATTC
ChIP_sll0814_F	Figure S5C #5	GTTACTACCGCTATCTATCG

ChIP_sll0814_R	Figure S5C #5	ATGACGTAAACCGGCTCTGAC
3Chox_Hcommon	Figure 5	CGGTCCCTTTGGACGTAATC
3Chox_H01_pos_+1	Figure 5	GGGTTGGGCGCAACATTAAG
3Chox_H02_pos_+3	Figure 5	CAAAGCGATTTTGGCTGGTG
3Chox_H03_pos_+4	Figure 5	GATGTGGTGGAAGATACGGAC
3Chox_H04_pos_+5	Figure 5	GGAGCCACAGGGGAATTTAAC
3Chox_H05_pos_+6	Figure 5	GGTCAGATTTTATTGGTTGCATGG
3Chox_H06_pos_+7	Figure 5	TTGTCAATGTCAACCGCAAC
3Chox_H07_pos_+8	Figure 5	TTATTGCCCAATCTGGCGAC
3Chox_H08_pos_+11	Figure 5	AGGCAAGACAGATAAACCTTCTG
3Chox_H09_pos_-2	Figure 5	GGGGCATAGGGAGCAAACC
3Chox_H10_pos_-4	Figure 5	GGGGTAGTACCGGAAGTGG
3Chox_H11_pos_-6	Figure 5	TTGGGCTGATTCTTGCAATTC
3Chox_H12_pos_-11	Figure 5	AGCTTTTGTCTAACACCGTATCG
3Chox_H13_pos_-13	Figure 5	AAGCCATCCTTCAAAACCCG
3Chox_H14_pos_-17	Figure 5	GCCCCATCGGTGAGAAAAAG
qPCR_hoxF_F	Figure 5 (internal control)	GTCATCTGCAATGCTGACGAA
qPCR_hoxF_R	Figure 5 (internal control)	CCAACACACTGCGGTCCAT